EFFECT OF THE DIRECTION OF THE ELECTRIC FIELD ON THE INTERFACIAL INSTABILITY BETWEEN A NEWTONIAN FLUID AND A VISCOELASTIC POLYMER

by

Aybike Nurocak

B.S., Chemical Engineering, Yıldız Technical University, 2009

Submitted to the Institute for Graduate Studies in
Science and Engineering in partial fulfillment of
the requirements for the degree of
Master of Science

Graduate Program in Chemical Engineering
Boğaziçi University

2012

to my father

ACKNOWLEDGEMENT

Apart from the efforts of myself, this thesis couldn't be accomplished without the encouragement and guidelines of many others. First of all, I wish to express my sincere gratitude to my thesis supervisor Assist. Prof. A. Kerem Uğuz for his tremendous support and help, invaluable assistance, and friendship.

I would like to thank Prof. Ramazan Yıldırım and Assoc. Prof. Hasan Bedir for the time they have devoted to reading and commenting on my thesis.

I wish to express my gratitude to all my friends for their support and their guidance through my graduate education. I would like to thank the members of KB 407 for their hospitality and helpfulness. I also thank my laboratory mate Dilek for her friendliness while we shared KB 406. I would like to thank all my class mates for helping and motivating me all the time.

Most importantly, I would like to express my very special thanks to my family. Above all, I am grateful to my father for his endless support in every part of my life, and especially for being my reason to be a chemical engineer. I would like to thank my mother for her invaluable love, patience and care. I am thankful to my lovely brother Alper for his sincere efforts to make me feel cheerful no matter how tired I am.

Finally, financial support provided by TÜBİTAK through project 109M557 is gratefully acknowledged.

ABSTRACT

EFFECT OF THE DIRECTION OF THE ELECTRIC FIELD ON THE INTERFACIAL INSTABILITY BETWEEN A NEWTONIAN FLUID AND A VISCOELASTIC POLYMER

Micro channels are widely used in many industrial applications as they offer the ability to work in small volumes, consume low energy and less time, and reduce costs. Another important application of microfluidics is to generate micro droplets of one phase in another immiscible phase and use them as reaction vessels. In order to generate droplets from these fluids, the interface needs to be stimulated. Electrohydrodynamics is an effective method for stimulating the interface in micro channels. The aim of this study is to analytically investigate the stability of the interface between a hydrodynamically passive fluid (air) and a viscoelastic polymer under the effect of an electric field applied either parallel or normal to the interface. By this analysis, the conditions for the interface deflection which is the first step of generating droplets are determined. The fluids are assumed to be immiscible, incompressible, and leaky-dielectric. The effect of using a passive fluid instead of an active one under the normal electric field, and the effect of the direction of the applied electric field are analyzed. As a result, it is found that the Weissenberg number for the system with passive fluid has an opposite effect on the maximum growth rate. Other dimensionless parameters such as the conductivity ratio, the dimensionless electric number, and the thickness ratio show the same trend in both the maximum growth rate, and the critical wave number. Moreover, for the given set of parameters, the system is always stable when a parallel electric field is applied. The neutral curves are also presented. For some values of dimensionless parameters, the solution failed and singularity occurred when the thickness ratio is 0.5 for the normal electric field. For the parallel electric field; no singularity occurred.

ÖZET

ELEKTRİK ALANI YÖNÜNÜN NEWTONYEN BİR AKIŞKAN İLE VİSKOELASTİK BİR POLİMERİN ARAYÜZEY KARARSIZLIĞINA ETKİSİ

Mikro kanallar küçük hacimlerde çalışma olanağı, daha az enerji ve zaman tüketimi, ve maliyette azalma sağladığından birçok endüstriyel uygulamalarda yaygın olarak kullanılmaktadırlar. Mikro kanallarda önemli bir diğer uygulama ise, bir fazın diğer karışmayan faz içinde mikro damlacık oluşturup reaksiyon hücresi olarak kullanmaktır. Bu sıvılarla damlacık oluşturmak için arayüzeyin uyarılması gerekmektedir. Elektrohidrodinamik uygulamalar mikro kanallarda iki karışmayan akışkan arasındaki arayüzeyi uyarmak için etkili bir yöntemdir. Bu çalışmanın amacı analitik olarak hem normal hem de paralel elektrik alan etkisinde hidrodinamik olarak pasif bir akışkan (hava) ve bir viskoelastik bir polimer arasındaki arayüzey kararsızlığını incelemektir. Bu analizle, damlacık oluşturmanın ilk adımı olan arayüzey bozulması için gereken koşullar belirlenir. Akışkanlar birbirleriyle karışmayan, sıkıştırılamaz, ve yarı yalıtkan olarak kabul edilmiştir. Aktif bir akışkanın yerine pasif bir akışkanın kullanılmasının etkisi, ve uygulanan elektrik alanın yönü incelenmiştir. Sonuç olarak, pasif bir akışkan kullanılan sistemin Weissenberg sayısının maksimum büyüme hızı üzerinde aktif bir akışkana göre tam ters bir etki yarattığı görülmüştür. İletkenlik oranı, boyutsuz elektrik sayısı, ve kalınlık oranı gibi diğer boyutsuz parametreler maksimum büyüme hızı ve kritik dalga sayısı üzerinde aynı eğilimi göstermişlerdir. Ayrıca paralel elektrik alan kullanıldığında kullanılan parametreler için sistem her zaman kararlıdır. Nötral eğriler de ayrıca sunulmuştur. Bazı boyutsuz parametre değerleri için çözüm hata vermiştir, ve normal elektrik alanda kalınlık oranı 0.5 iken düzensizlik oluşmuştur. Paralel elektrik alan kullanıldığında herhangi bir düzensizlik oluşmamıştır.

TABLE OF CONTENTS

LIST OF FIGURES

LIST OF TABLES

LIST OF SYMBOLS

$2\underline{\underline{D}}$	shear rate of the fluid
2H	twice the surface mean curvature
De	Deborah number
$\underline{E}$	electric field
E_b	dimensionless electric number
f	constant surface
G	rigidity modulus
$h^{(j)}$	fluid thickness for the j^{th} phase
H_r	thickness ratio
k	consistency of the fluid (at non-Newtonian models)
k	wave number (at modeling)
k_c	critical wave number
k_{max}	wave length of the fastest growing mode
L	length of the channel
n	power law index
$\underline{n}$	unit normal vector
p	pressure
q	surface charge density
q_t	time derivative of the charge density
Re	Reynolds number
S	the ratio of the fluid to electric time scale
s_{max}	maximum growth rate of the fastest growing mode
$\underline{t}$	unit tangent vector
$\underline{\underline{T}}$	total stress tensor
t_E	electric time scale
t_F	fluid time scale
u	normal speed of the interface
$\underline{u_s}$	surface velocity
$\underline{v}$	velocity

V	voltage
V_b	applied voltage
We	Weissenberg number
$\overline{x}$	overbar: dimension of the variables
$\tilde{x}$	tilde: dimensionless parameter
x_0	subscript 0: base state parameter
x_1	subscript 1: perturbed state parameter
z_1	mapping from the reference domain to current domain
β	ratio of the depth of the bottom layer to channel length
γ	relaxation time (for non-Newtonian models)
$\dot{\gamma}$	shear rate
∇	gradient
∇_s	surface gradient
ε	relative permittivity
ε_0	vacuum permittivity
ϵ	an infinitesimally small perturbation
λ_1	relaxation time
λ_2	retardation time
μ_0	total viscosity
μ_a	apparent viscosity
μ_p	polymer viscosity
Π	derivation operator
ρ	density
σ	electrical conductivity
σ_r	electrical conductivity ratio
$\underline{\underline{\tau}}$	viscous stress tensor
$\underline{\underline{\tau}}^p_{(1)}$	convective derivative of the stress tensor
$\underline{\underline{\tau}}^p$	polymeric contribution to the stress
$\underline{\underline{\tau}}^s$	solvent contribution to the stress
τ_y	yield stress

ω	growth rate constant

LIST OF ACRONYMS/ ABBREVIATIONS

AC	alternating current
DC	direct current
LISA	lithographically induced self assembly
NSB	normal stress balance
PDMS	polydimethylsiloxane
PMMA	poly methyl methacrylate
PS	polystyrene
TSB	tangential stress balance
UCM	upper convective Maxwell

1. INTRODUCTION

Microfluidics is becoming increasingly important in recent years due to the development of lab-on-a-chip devices, i.e., systems that are able to perform a large number of tasks on small chips, such as mixing, separating, driving fluids, and, analyzing and detecting molecules (Whitesides, 2006; Tabeling, 2001). Lab-on-a-chip provides a technology that process small (microliter to picoliter) amounts of fluids and, offers the ability to study in small volumes, consume low energy and less time, and reduce costs. However, those devices have some drawbacks such as mixing. Mixing is required in many systems such as biochemistry analysis, drug delivery, sequencing or synthesis of nucleic acids, and also complex chemical reactions (Nyugen and Wu, 2005). On large scales, fluids mix convectively; however, in microsystems, when two fluid streams come together, they flow in parallel; the flow is laminar without eddies or turbulence, and occurs at low Reynolds number (Whitesides, 2006). In order to achieve mixing, some passive mixing methods such as changing the geometry (Hosokawa *et al*., 1999; Liu *et al*., 2000; Nyungen and Wu, 2005; Sudarsan and Ugaz, 2006; Stroock *et al*., 2002; Howell *et al*., 2005; Kim *et al*., 2004) to increase the contact surface area and decrease the diffusion path, and some active mixing methods such as generation of pulsing velocity (Deshmukh *et* al., 2000; Glasgow and Aubry, 2003) are employed.

In micro scales, there is another challenge except mixing which is the formation of droplets. Multiphase flows enable the generation of droplets of a dispersed gas or liquid phase in a continuous liquid stream, and they can be used in the production of polymer particles, emulsions, or foams (Whitesides, 2006). The potential applications of droplet-based microfluidics in various fields such as chemical or biochemical analysis, fabrication of micro particles, the formation and manipulation of micro droplets are receiving increased interest from researchers worldwide. Passive methods relying mostly on channel geometry (Anna *et al*., 2003; Stroock *et al*., 2002; Dasgupta *et al*., 2001) have been used to form micro droplets; however, the size of the droplet cannot be controlled directly. The droplets with different size can cause some technical problems; for instance, especially in drug delivery systems, mono dispersed droplet size is crucial (Ozen *et al*., 2006a).

Lately, external electric field is used for forming mono sized micro droplets for immiscible fluids, or for efficient mixing of miscible fluids in micro channels. Electrohydrodynamics deals with fluid motion induced by electric fields. If the electrical force's magnitude is large enough, it creates a transversal secondary flow across the interface, thus destabilizing the interface and promoting the mixing process (Moctar *et al*., 2003). Applying an electric field has the advantage that the electric signals can be easily controlled; hence, the size of the droplets can be controlled (Choi *et al*., 2011).

Non-Newtonian fluids have an important part in chemical industry; however, there are few works which investigate their stability. After the lithographically-induced self-assembly (LISA) process (Chou and Zhuang, 1999) has emerged, the polymer-air system under the effect of an applied electric field has become widespread (Schäffer *et al*., 2001; Salac *et al*., 2004; Harkema *et al*., 2003). There are few works which analyze the stability of the interface of a viscoelastic polymer which is one of the important non-Newtonian fluid/air system under a normal electric field (Wu and Chou, 2005; Tomar *et al*., 2007); however, the stability of the interface of a viscoelastic polymer and air system under a parallel electric field has not been analyzed yet.

In this work, the stability of the interface between a viscoelastic polymer and air under the effect of an externally applied normal and parallel electric field is studied. The Upper Convected Maxwell (UCM) model is used for the viscoelastic polymer, and linear stability analysis is applied. The effect of the direction of the electric field on the stability of the interface is analyzed for various parameters such as thickness ratio, applied voltage, and Weissenberg number.

2. LITERATURE SURVEY

2.1. Physical System

In many micro systems, the effect of gravity is neglected (Ozen *et al*., 2006b; Shankar and Sharma, 2004; Craster and Matar; 2005) since the fluids' thickness are very thin in micro channels. Different base state profiles are assumed. Yiantsios and Higgins (1988), Uguz and Aubry (2008), Talon and Meiburg (2001) assumed the base state flow profiles as Poiseuille flow, i.e. pressure driven flow. They all considered bounded geometry with no-slip walls. On the other hand; Abdella and Rasmussen (1997), Mahlmann and Papageorgiou (2011), and Shankar and Kumar (2004) assumed the base state profiles as Couette flow which is driven by moving the wall at a constant speed. Furthermore; some other studies assumed stationary base state (Shankar and Sharma, 2004; Craster and Matar; 2005). Li *et al*. (2007) carried out a study with both the Poiseuille flow and the Couette flow; they found that the results do not depend on the base state profiles.

There are two different common modeling about the interfacial instability between two fluids under the influence of an electric field. These are the "bulk-coupled model" and the "surface-coupled model". A conductivity gradient at the interface is assumed for the bulk coupled model. An electrical force occurs in the bulk of the fluids due to the close values of the electrical properties of the fluids at the interface. Hoburg and Melcher (1976) used such a model to study the effect of a conductivity gradient on the stability of two fluids under the effect of a parallel electric field. On the other hand, the surface coupled model considers a jump in the electrical conductivity at the interface, and there are no electrical forces present in the fluids. Therefore, there are no electric forces in the governing equations (Ozen *et al*., 2006b; Uguz *et al*., 2008). Melcher and Schwarz (1968) used surface coupled model to study the stability of two fluids subjected to a normal electric field. The latter studies and this thesis consider the surface coupled model.

In some studies, the fluid flow characteristic time scale is assumed to be very large with respect to the electrical charge relaxation time, so the ratio of fluid time scale to electric time scale, S, is very large, which is called "the fast electric time". This large S led

to a considerable simplification of the equations (Pease and Russel, 2002; Li et al., 2007; Ozen et al., 2006a; Ozen et al., 2006b). Uguz and Aubry (2008) and Uguz *et al.* (2008) assumed large S to determine the stabilizing/destabilizing regions in the conductivity versus permittivity ratio plane without actually solving the equations. Ozen *et al*. (2006b) studied the effect of S, and they found that the critical wave number decreases, and the maximum growth rate stays constant while S increases.

Pease and Russel (2002) used linear stability analysis to investigate the effects of various process parameters, specially the conductivity, and the film thickness. Guo *et al.* (2002) performed a linear stability analysis, and a non-linear stability analysis to investigate the interface of a stratified gas–liquid two-phase flow in a circular pipe. The non-linear stability analysis verified the conclusions reached by the linear stability analysis which is used to decide on the stability of the interface and gave information about the growth and propagation of the interfacial disturbances (Guo *et al*., 2002).

On the other hand, Thaokar and Kumaran (2005) used weakly non-linear analysis, thin film analysis, and a boundary integral method. The weakly non-linear analysis enables to examine the effect of the non-linear interactions on the evolution of the initial perturbation. The thin film analysis is also called the “long wave analysis”, or the “lubrication theory” as the wave length of perturbations is large compared to the film thickness. When the film thickness is comparable to the wave length of the perturbation, the boundary integral method is used, and is applicable to zero Reynolds flow (Thaokar and Kumaran, 2005). Craster and Matar (2005) used lubrication theory to analyze the stability between two thin leaky-dielectric liquid films sandwiched between two infinitely long, rigid and impermeable electrodes. They derived non-linear partial differential equations to describe the growth of the interfacial deflection and the surface charge density. They found that decreasing the thickness ratio and the viscosity ratio has a destabilizing effect.

2.1.1. Electrical Conductivity

The electrical conductivity of the fluids is an essential parameter for the modeling of the system. If the fluids are not conductive, either “perfect dielectric” or “leaky dielectric” model is used. Perfect dielectrics have zero conductivity, and there are no free charges. “Leaky dielectric” model, which was proposed by Taylor and Melcher (1969), hence also called the "Taylor-Melcher leaky dielectric model" assumes non-zero uniform conductivity for the fluids.

Leaky dielectric model as it allows even a slightness of conductivity, is widely used to investigate interfacial instabilities in the presence of an electric field (Burcham and Saville, 2000; Li *et al*., 2007; Ozen *et al*., 2006b; Uguz *et al*.., 2008; Khorshidi *et al*., 2011; Uguz and Aubry, 2008). Khorshidi *et al*. (2011) have studied the response of the interface between two leaky dielectric fluid layers exposed to external uniform and non-uniform electric fields. They demonstrated that applying an external electric field, higher than the critical value, causes fluctuations at the interface, and reaches to an instability at the interface (Khorshidi *et al*., 2011). Ozen *et al.* (2006b) performed stability analysis of a system of two leaky dielectric fluids in plane Poiseuille flow, and they found that the electric field can be either stabilizing or destabilizing, and all the ratios of electrical and mechanical properties have a significant effect on both the maximum growth rate and the critical wave number.

Schäffer *et al*. (2000) investigated the instability of the interface between a perfect dielectric fluid and air, Lin *et al*. (2001), and, Thaokar and Kumaran (2005) studied the interfacial instability of the system with both two perfect dielectric fluids and two leaky dielectric fluids under the effect of an electric field. They found that the critical potential for the leaky dielectrics is smaller than that for the perfect dielectrics to destabilize the system. Pease and Russel (2002) studied a system with two perfect dielectric fluids, and the same system with one perfect dielectric fluid and one leaky dielectric fluid. They concluded that the growth rate and the characteristic wave number in leaky dielectric-perfect dielectric fluid system are much larger than that for the two perfect dielectric fluids system.

2.1.2. Alternating or Direct Current

The direction of the current is periodically being reversed back and forth for an alternating current (AC); whereas it flows only in one direction for a direct current (DC). Most of the studies are carried out with DC electric field; however there are few works attributed to the AC field (Dong *et al*., 2001; Mohring *et al*., 2003; Robinson *et al*., 2001; Roberts and Kumar, 2009; Gambhire and Thaokar, 2010; Gambhire and Thaokar, 2011).

Roberts and Kumar (2009) studied the stability of the interface between two perfect dielectrics and two leaky dielectric fluids under the effect of the AC field, and, then they compared the results with the DC field. For perfect dielectrics, they found that s_{max}, the maximum growth rate of the fastest growing mode, and k_{max}, the wave length of the fastest growing mode, are smaller for the AC field than that for the DC field. The electric field frequency has an imperative effect on the growth of interfacial charge, and this can be used to adjust the instability growth rate, and the wave number (Roberts and Kumar, 2009).

Gambhire and Thaokar (2011) studied the effect of the AC and the DC electric fields on the stability of the interface between a perfect dielectric fluid and a leaky dielectric fluid, and two perfect dielectrics. They showed that varying the conductivity of the perfect dielectric fluid does not change the growth rate significantly in the DC field for perfect dielectric-leaky dielectric system. However, in the AC field, this dependence increases at intermediate frequencies. For perfect dielectric fluids, they showed that the AC field does not have an impact on the growth rate compared to the DC field. In this study, the DC electric field is used.

2.1.3. Direction of the Electric Field

In electrohydrodynamic studies, the electric field could be applied normal (Kath and Hoburg; 1977; Abdella and Rasmussen, 1997; Belonozkho *et al*., 1998; Pease and Russel, 2002; Shankar and Sharma, 2004) or parallel (Papageorgiou and Petropoulos, 2004; Patankar, 2011; Uguz *et al*., 2008; Uguz and Aubry, 2008) to the interface between the fluids. Kath and Hoburg (1977) investigated the instability at the interface between two miscible fluids with identical permittivity, density, and viscosity but different

conductivities under the effect of a normal electric field. One of the reason for the use of parallel electric field is the observed wave length in the channel depends on the length of the electrodes. During an experiment, if the wave lengths are longer than the electrodes, the results can be misleading. On the other hand; parallel field's electrodes are located at two edges of the channel so any wave length can be observed in the channel. Ozen *et al*. (2006) studied the linear stability of the interface between two leaky dielectric fluids with different permittivities and conductivities subjected to a normal electric field. They concluded that all of the electrical and mechanical properties of the two fluids have an important effect on both the maximum growth rate and the critical wave number. The effect of a parallel electric field on the interface is also investigated (Papageorgiou and Petropoulos, 2004; Patankar, 2011; Uguz *et al*., 2008; Uguz and Aubry, 2008). Papageorgiou and Petropoulos (2004) studied the stability of the initially flat interface of an incompressible conducting liquid film surrounded by a passive conducting medium under the effect of a parallel electric field. They showed that the magnitude of the product of conductivity and permittivity ratio decide whether the interface is stable or not. Uguz *et al*. (2008) compared analytically the effect of the parallel electric field to that of the normal electric field on the stability of the interface of two leaky-dielectric fluids in a micro channel. They plotted the permittivity ratio versus conductivity ratio, and determined regions where the parallel or the normal electric field has a stabilizing or destabilizing effects. They found that the normal electric field causes instability for a broader range of the parameters than the parallel field. In the current study, both the normal and the parallel electric fields are studied, and compared.

2.2. Non-Newtonian Fluid Properties and Modeling

In electrohydrodynamic instability studies, recently polymers have been used more often especially after the introduction of the LISA (lithographically-induced self-assembly) process (Chou and Zhuang, 1999). For polymer solutions and polymer melts the stress-strain relationship is usually described with a nonlinear equation, i.e. a non-Newtonian constitutive equation. Therefore, modeling of non-Newtonian fluids is explained in this section.

The flow curve of a non-Newtonian fluid is not linear due to an unstable viscosity at a given pressure, and temperature (Wilkinson, 1960). There are three types of non-Newtonian fluids as time-independent, time-dependent, and viscoelastic fluids.

2.2.1. Time-independent Non-Newtonian Fluids

The shear rate at any point is defined only by the corresponding current value of the shear stress for time-independent fluids (Chhabra, 2008).

$$\dot{\gamma}_{yx} = f(\tau_{yx}) \tag{2.1}$$

These fluids can be subdivided into three groups as Bingham plastics, pseudoplastic fluids, and dilatant fluids.

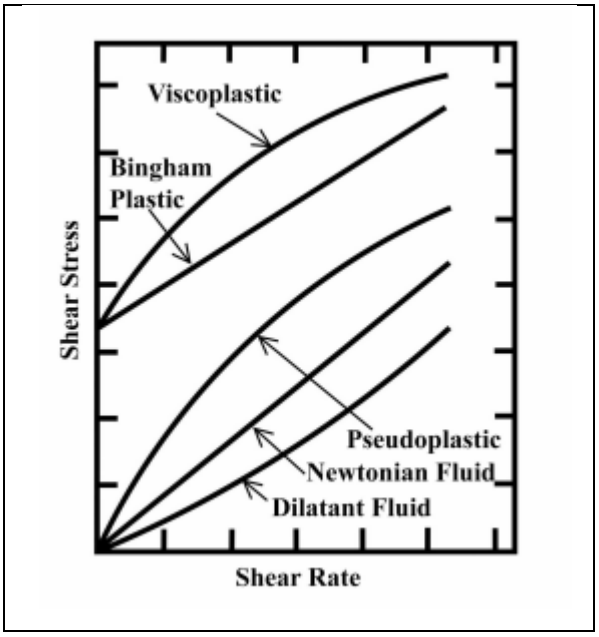

Figure 2.1. Flow curves for different types of non-Newtonian fluids
(This figure was published in 2008, Chhabra, R. P., and J. F. Richardson, Non-Newtonian Flow and Applied Rheology, 2nd ed., pp.6, Copyright Elsevier).

2.2.1.1. Bingham plastics. Bingham plastics are viscoplastic fluids which behave like a rigid body at rest. They need to exceed the yield stress, τ_y, to be able to flow. τ_y is defined as the intercept on the shear stress axis of the Bingham plastics curve (Figure 2.1). Many fluids, such as tomato paste, slurries, oil paints, toothpaste, mayonnaise, are examples of Bingham plastics. The rheological equations for these types of fluids are as follows:

- The Bingham plastic model.

$$\tau_{yx} = \tau_y + \mu_p \dot{\gamma}_{yx} \;\; ; \;\; |\tau_{yx}| > |\tau_y| \tag{2.2}$$

$$\dot{\gamma}_{yx} = 0 \; ; \;\; |\tau_{yx}| < |\tau_y| \tag{2.3}$$

where τ_{yx} is shear stress, τ_y is the yield stress, μ_p is the plastic viscosity, and $\dot{\gamma}_{yx}$ is the shear rate.

- The Herschel- Bulkley model.

$$\tau_{yx} = \tau_y + \; k(\dot{\gamma}_{yx})^{\,n} \;\; ; \;\; |\tau_{yx}| > |\tau_y| \tag{2.4}$$

$$\dot{\gamma}_{yx} = 0 \; ; \;\; |\tau_{yx}| < |\tau_y| \tag{2.5}$$

where k is a measure of the consistency of the fluid, higher k means more viscous fluids, and n is a measure of the degree of non-Newtonian behavior.

- The Casson model.

This model is mainly derived for modeling the flow of blood, but it is a good approximation also for other substances.

$$\sqrt{|\tau_{yx}|} = \sqrt{\tau_y} + \sqrt{\mu_p |\dot{\gamma}_{yx}|} \; ; \;\; |\tau_{yx}| > |\tau_y| \tag{2.6}$$

$$\dot{\gamma}_{yx} = 0\ ;\ \ |\tau_{yx}| < |\tau_y| \tag{2.7}$$

2.2.1.2. Pseudoplastic fluids. These types of fluids' apparent viscosity, μ_a, gradually decreases with an increase in the rate of shear, and the flow curve becomes linear only at very high rates of shear. The apparent viscosity is defined as

$$\mu_a = \frac{\tau_{yx}}{\dot{\gamma}_{yx}} \tag{2.8}$$

or

$$\mu_a = k\left(\dot{\gamma}_{yx}\right)^{n-1} \tag{2.9}$$

For n < 1, the fluid shows shear-thinning behavior, for n = 1, the fluid shows Newtonian behavior, for n > 1, the fluid shows shear-thickening behavior.

In these equations, k and n are fluid consistency coefficient, and the flow behavior index, respectively. For these types, the plot of shear stress and rate of shear is often found to be linear with a slope between zero, and unity (Wilkinson, 1960; Chhabra, 2008). Therefore, the power law relation is most widely used, and the most common example of pseudoplastic fluid is paint.

- Power law or Ostwald de Waele equation:

$$\tau_{yx} = k(\dot{\gamma}_{yx})^{\,n} \tag{2.10}$$

where k, and n are constants which n is between zero and unity. The fluids with smaller value of n exhibit more shear thinning behavior. The constant, k, is a measure of consistency of the substance (Chhabra, 2008).

2.2.1.3. Dilatant Fluids. The viscosity of dilatant fluids increases with increasing shear rate, and they do not show yield stress. Therefore, they are also called shear thickening. The power law model can be applied also for these fluids, but the constant n is greater than unity. Starch pastes are the most common examples of this type (Wilkinson, 1960).

2.2.2. Time-dependent Non-Newtonian Fluids

The viscosity of time-dependent non-Newtonian fluids depends not only shear rate, and shear stress, but also on the time the shear has been applied. These fluids may be grouped as thixotropic, and rheopectic fluids.

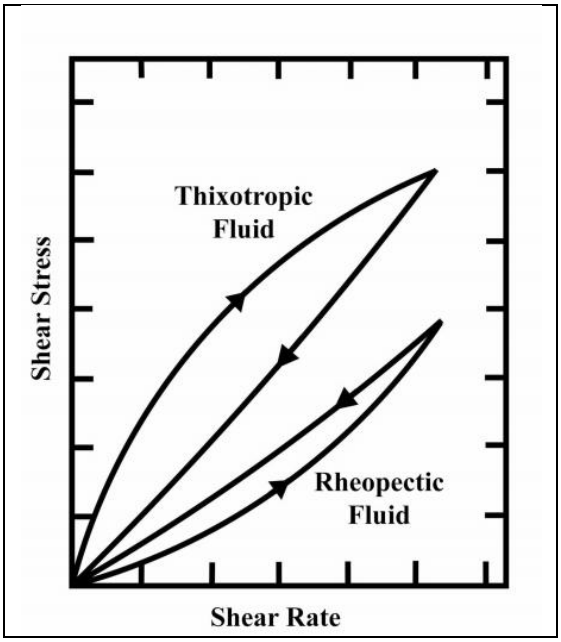

Figure 2.2. Shear stress versus shear rate plot for thixotropic and rheopectic fluids (This figure was published in 2008, Chhabra, R. P., and J. F. Richardson, Non-Newtonian Flow and Applied Rheology, 2nd ed., pp.6, Copyright Elsevier).

2.2.2.1. Thixotropic Fluids. The apparent viscosity of thixotropic fluids depends on the duration of shearing. If a thixotropic fluid is sheared at a constant rate, the apparent viscosity will decrease with time, as seen in Figure 2.2 (Wilkinson, 1960).

2.2.2.2. Rheopectic Fluids. Rheopectic fluids, in contrast to thixotropic fluids, show a behavior that their apparent viscosity increases with time of shearing, as seen in Figure 2.2 (Chhabra, 2008).

2.2.3. Viscoelastic Fluids

Viscous materials resist shear flow linearly with time, and elastic materials recover instantaneously their original state when the stress is removed. Viscoelastic fluids have both elastic, and viscous properties at the same time, and viscoelastic fluids are assumed as time dependent, as their viscosity is time dependent. So, the rheological equation of this type of fluids is obtained by taking the time derivative of Equation (2.1) as (Wilkinson, 1960)

$$f_1\left(\frac{d\tau_{yx}}{dt}\right) = f_2\left(\frac{d\dot{\gamma}_{yx}}{dt}\right) \tag{2.11}$$

Equation (2.11) is a general equation for viscoelastic fluids; it should be solved subject to the appropriate boundary conditions to obtain the response of the material to any applied stress or strain. But for real fluids, it is very difficult to solve that equation and their behavior can be characterized by a single parameter using mechanical models. These models contain dash-pot and spring system. Dash-pot represents the viscous properties, and spring represents the elastic properties of the fluid (Wilkinson, 1960).

2.2.3.1. Voigt model. This model is a parallel combination of dash-pot, and spring (Wilkinson, 1960). The behavior of the fluid in shear is given by

$$\tau_{yx} = G\,\gamma_{yx} + \mu\,\dot{\gamma}_{yx} \tag{2.12}$$

where G is a rigidity modulus (spring constant). Integrating Equation (2.12) gives

$$\gamma_{yx} = exp\left(-\frac{G}{\mu}t\right)\left[\gamma_0 + \frac{1}{\mu}\int \tau_{yx}\, exp\left(\frac{G}{\mu}t\right)dt\right] \tag{2.13}$$

where γ_0 is the strain at time, t=0.

2.2.3.2. Maxwell model. This model is composed of dash-pot, and spring in series. The equation for this model is (Wilkinson, 1960)

$$\dot{\gamma}_{yx} = \frac{\dot{\tau}_{yx}}{G} + \frac{\tau_{yx}}{\mu} \tag{2.14}$$

where the " ˙ " symbol represents the time derivative. Integrating Equation (2.14) gives

$$\tau_{yx} = exp\left(-\frac{G}{\mu}t\right)\left[\tau_0 + G\int \gamma\, exp\left(\frac{G}{\mu}t\right)dt\right] \tag{2.15}$$

where $\gamma = \mu/G$ is the relaxation time.

2.2.3.3. Jeffreys model. This model includes time derivative of the velocity gradients in Maxwell model (Bird *et al*., 2007).

$$\underline{\underline{\tau}} + \lambda_1 \frac{\partial \underline{\underline{\tau}}}{\partial t} = \mu_0(\underline{\underline{\dot{\gamma}}} + \lambda_2 \frac{\partial \underline{\underline{\dot{\gamma}}}}{\partial t}) \tag{2.16}$$

where λ_1 is the relaxation time, and λ_2 is the retardation time.

2.2.3.4. Oldroyd-B model. This model is derived from Equation (2.16) replacing time derivatives with upper convected time derivatives.

$$\underline{\underline{\tau}} + \lambda_1 \underline{\underline{\tau}}_{(1)} = \mu_0(\underline{\underline{\gamma}}_{(1)} + \lambda_2 \underline{\underline{\gamma}}_{(2)}) \tag{2.17}$$

where μ_0 is the total viscosity which consists of solvent, and polymer viscosity, $\underline{\underline{\gamma}}_{(1)}$ and $\underline{\underline{\gamma}}_{(2)}$ are the convective derivatives of shear rates, $\underline{\underline{\tau}}_{(1)}$ represents convected derivative of the stress tensor, λ_1 is the relaxation time, and λ_2 is the retardation time. The definition of the upper convected time derivate is

$$\underline{\underline{\tau}}_{(1)} = \frac{D}{Dt}\underline{\underline{\tau}} - \{(\nabla v)^T \cdot \underline{\underline{\tau}} + \underline{\underline{\tau}} \cdot \nabla \underline{v}\} \tag{2.18}$$

where the superscript T stands for the transpose and D/Dt for the material derivative. The upper convected time derivative is the variation of some tensor property of fluid with time following translation, rotation, and deformation of material. This model reduces to a purely viscous Newtonian fluid if λ_1=λ_2 (Darby, 1976). If the solvent viscosity is zero, the Oldroyd-B becomes Upper Convected Maxwell (UCM) model (Owens and Philips, 2002). Common examples of UCM type fluids are polymer solution and melts, oil, toothpaste, and clay.

In this work, Upper Convected Maxwell (UCM) model is accepted as a constitutive equation.

2.2.3.5. Oldroyd 3-constant model (Kopaç *et al.*, 1998).

$$(1 + \lambda_1\, \Pi)\underline{\underline{\tau}} = -2\mu(1 + \lambda_2\, \Pi)\underline{\underline{\dot{\gamma}}} \tag{2.19}$$

where Π is a derivation operator, λ_1 and λ_2 are first, and second time constants, respectively.

2.2.3.6. Kopaç-Arıkol model (Kopaç *et al.*, 1998).

$$\left(1 + \lambda\, \Pi\left(\underline{\underline{\dot{\gamma}}}\right)\right)\underline{\underline{\tau}} = -2\mu\left(1 + \lambda\, \Pi\left(\underline{\underline{\dot{\gamma}}}\right)\right)\underline{\underline{\dot{\gamma}}} \tag{2.20}$$

where λ, and μ are defined as

$$\lambda = \frac{1}{\lambda_0 + \lambda_1|\Pi|^{r/2}} \tag{2.21}$$

$$\mu = \frac{\mu_0}{1 + d_1|\Pi|^{r/2}} \tag{2.22}$$

where λ_0, λ_1, d_1 and r are constant parameters related to relaxation time and viscosity (Kopaç *et al.*, 1998).

2.3. Non-Newtonian Fluids in Electrohydrodynamic Instabilities

The self assembly of polymeric microstructures is an important innovation that technologically presents low cost and high efficiency. Chou and Zhuang (1999) introduced the lithographically induced self-assembly (LISA) process, for the first time. In LISA, a thin polymer film is first applied on to a flat substrate and then a mask is placed above the film. The system is heated uniformly above the glass transition temperature of the polymer and then is cooled down to room temperature. During this cycle, the polymer rises up against the gravitational force, and the surface tension, and the pillars are formed. The shapes of the pillars depend on many parameters such as the physical and the electrical properties of the polymer, and the channel thickness (Chou and Zhuang, 1999). After the LISA process (Chou and Zhuang, 1999), there is an increasing interest in this field. The polymer-air, and the polymer-polymer interface under the effect of an electric field are studied (Schäffer *et al.*, 2000; Leach *et al.*, 2005; Salac *et al.*, 2004; Pease and Russel, 2002; Balmforth *et al.*, 2003). They found patterns similar to those observed in the LISA process. Schäffer *et al*. (2000) performed an experiment to investigate the instability of the polymer-air interface between two electrodes under the effect of an electric field. The result of the experiment showed that the columnar structures were formed at the higher electric part of the electrode, thus the instability increases as the electric field strength increases. Apart from these polymer-air systems, Leach *et al*. (2005) studied a trilayer thin film system consisting of two different polymers; polymethyl methacrylate (PMMA) and polystyrene (PS), and air under a normal electric field to the interface. As a result, the electrostatic forces, and the dewetting forces at two interfaces played an important role in type of structures obtained. When PS was used, the polymer interface was destabilized, and lead to the formation of columnar structures. The pillars had a PS core with a PMMA sheath, by selectively removing the PS core, hollow structures can also be obtained.

The non-Newtonian behavior of the polymers is first studied by Eldabe (1987) who investigated the instability of two dielectric polymeric fluids between two infinitely long

electrodes under the effect of a normal electric field. The fluids assumed Couette flow, and the power law was used as a constitutive equation. The results of the linear stability analysis showed that the system can be unstable depending on the electric field strength, the thickness of the channel, the viscosities, and the power law indexes of the fluid. Wu and Chou (2005) performed a linear stability analysis to a system of a viscoelastic polymer film and air under a mask subjected to a normal electric field. They assumed viscoelastic polymer as a leaky dielectric fluid, and they used Oldroyd-B model as a constitutive equation. The Oldroyd-B model reduced to Jeffreys model, under the lubrication assumption. The polymer is a Maxwell fluid so the solvent viscosity is zero. The base state interface is stationary, and the air is totally stationary. The inertial effects are ignored, and Stokes equation is employed. They found that the growth rate increases with the Deborah number, De. When De is below a critical value, the elasticity increases the growth rate without affecting the most dangerous wave number. When De is above the critical value, infinitely large growth rate occurs. The elasticity increases the growth rate without affecting the most dangerous wave number when De is below a critical value. When De is above the critical value, the resonance (infinitely large growth rate) occurs. The resonance is affected by the viscoelasticity and the dimensionless film thickness of the polymer, but the electrical properties of the polymer do not affect the resonance (Wu and Chou, 2005). Tomar *et al.* (2007) investigated the reasons of the resonances in the work of Wu and Chou (2005). They worked with the same system with and without the solvent viscosity and with and without the inertial effects using the full dispersion relation. They performed linear stability analysis without the long wave assumption. They found similar results in the absence of inertia and solvent viscosity. In the presence of inertia and solvent viscosity, they found that above a critical De, De_c, the growth rate is large but not infinite. Pinarbasi and Liakopoulos (1995) performed a linear stability analysis of the interface between two non-Newtonian inelastic fluids in a straight channel driven by a pressure gradient. Two distinct models are studied; Bingham-like fluids, and Carreau-Yasuda fluids. They started the experiments with two Newtonian fluids and then replaced the bottom fluid with a viscoplastic fluid; this change leads a stabilizing effect on the interface for intermediate and large wave numbers. In the case of two non-Newtonian fluids, they showed that zero-shear-rate viscosity ratio destabilizes the flow.

3. THE PHYSICAL SYSTEM AND THE MODELING EQUATIONS

The stability of the interface is analyzed for two different cases, under the effect of a normal and a parallel electric field, respectively. First, the equations of the system under the effect of a normal electric field are derived and then the equations of the same system under the effect of a parallel field are introduced.

3.1. A Non-Newtonian Fluid and Air System Under the Influence of a Normal Electric Field

The interfacial instability of two incompressible, leaky-dielectric, immiscible, and non-reactive fluids is analyzed under the effect of a normal electric field. The fluid, denoted with superscript 1, is a non-Newtonian polymer, and the other fluid denoted with superscript 2 is air. The physical system is depicted in Figure 3.1.

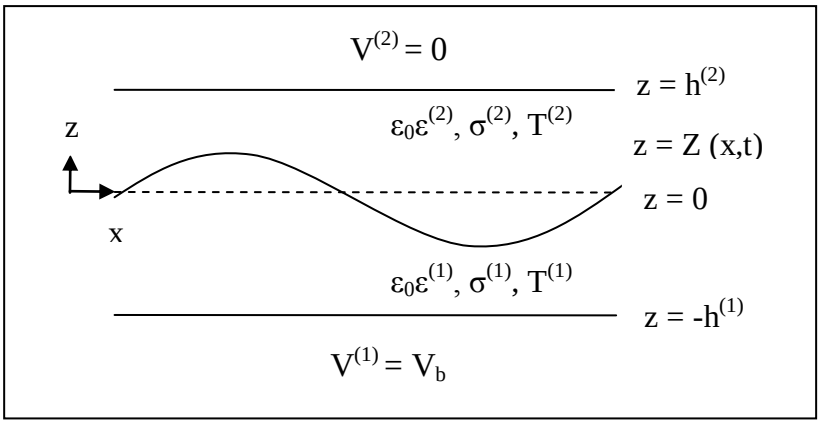

Figure 3.1. Two-phase system under the effect of normal electric field

The first fluid whose electrical permittivity, $\varepsilon_0\varepsilon^{(1)}$, conductivity, $\sigma^{(1)}$, total stress tensor, $T^{(1)}$ is a non-Newtonian viscoelastic polymer. The second fluid whose electrical permittivity, $\varepsilon_0\varepsilon^{(2)}$, conductivity, $\sigma^{(2)}$, total stress tensor, $T^{(2)}$ is air which is assumed to be hydrodynamically passive. An electric field is applied in the normal direction to the flat interface with a potential V_b at the lower wall located at $z = -h^{(1)}$, and the upper wall located at $z = h^{(2)}$ is grounded.

3.1.1. Governing Equations

There are no electric forces in the governing equations due to the surface-coupled model that is employed (Uguz *et al.*, 2008). Electric forces appear only at the boundary and the interface conditions. Since the second fluid, i.e. air, is stationary, $\underline{v}$ represents only the second fluid's velocity, and the superscript is omitted.

For the first fluid, located at $-h^{(1)} < z < Z(x,t)$, the equation of motion is

$$\rho\left[\frac{\partial \underline{v}}{\partial t} + \underline{v}.\nabla\underline{v}\right] = -\nabla p + \nabla.\underline{\underline{\tau}} \tag{3.1}$$

the continuity equation for an incompressible fluid is

$$\nabla.\underline{v} = 0 \tag{3.2}$$

and the Laplace equation for the electric field is given as follows

$$\nabla^2 V^{(1)} = 0 \tag{3.3}$$

Here $\underline{v}$, p, V, and $\underline{\underline{\tau}}$ represent velocity, pressure, voltage, and viscous stress tensor for the first fluid, respectively. The second fluid, air, is passive; therefore, the equation of motion, and the continuity equation are not needed. Laplace equation for the second fluid, located at $Z(x,t) < z < h^{(2)}$, is

$$\nabla^2 V^{(2)} = 0 \tag{3.4}$$

For the Oldroyd-B model, the shear stress is given by

$$\underline{\underline{\tau}} = \underline{\underline{\tau}}^p + \underline{\underline{\tau}}^s \tag{3.5}$$

where $\underline{\underline{\tau}}^p$, and $\underline{\underline{\tau}}^s$ are the polymeric contribution, and the viscous solvent contribution to the stress, respectively (Bird *et al*., 1987; Shaqfeh *et al*., 1989) defined as

$$\lambda \underline{\underline{\tau}}^p_{(1)} + \underline{\underline{\tau}}^p = \mu_p 2\underline{\underline{D}} \tag{3.6}$$

$$\underline{\underline{\tau}}^s = \mu_s 2\underline{\underline{D}} \tag{3.7}$$

respectively. Here, μ_p is the polymeric contribution, μ_s is the solvent contribution to the shear viscosity, λ is the relaxation time of the polymer, $2\underline{\underline{D}}$ is the shear rate of the fluid, and $\underline{\underline{\tau}}^p_{(1)}$ is the convective derivative of the stress tensor, which is given by

$$\underline{\underline{\tau}}^p_{(1)} = \frac{D}{Dt}\underline{\underline{\tau}}^p - \{(\nabla v)^T \cdot \underline{\underline{\tau}}^p + \underline{\underline{\tau}}^p \cdot \nabla \underline{v}\} \tag{3.8}$$

Here, the superscript T stands for the transpose. The material derivate is expanded, and inserted in Equation (3.8) as

$$\underline{\underline{\tau}}^p_{(1)} = \frac{\partial}{\partial t}\underline{\underline{\tau}}^p + \underline{v} \cdot \nabla \underline{\underline{\tau}}^p - (\nabla v)^T \cdot \underline{\underline{\tau}}^p - \underline{\underline{\tau}}^p \cdot \nabla \underline{v} \tag{3.9}$$

The component form of Equation (3.9) is

$$\underline{\underline{\tau}}^p_{(1)} = \frac{\Delta \tau^p_{ij}}{\Delta t} \equiv \frac{\partial \tau^p_{ij}}{\partial t} + v_k \frac{\partial \tau^p_{ij}}{\partial x_k} - L_{jk}\tau^p_{ki} - L_{ik}\tau^p_{kj} \tag{3.10}$$

where L_{ij} is defined as follows:

$$L_{ij} = \frac{\partial v_i}{\partial x_j} \tag{3.11}$$

For the Newtonian fluids, $\mu_p = 0$, and for the Upper Convective Maxwell (UCM) model, $\mu_s = 0$. In this work, UCM model is assumed, therefore the shear stress of the fluid depends only on the polymer viscosity (Bird *et al*.,1987; Denn, 1990).

$$\underline{\underline{\tau}} = \underline{\underline{\tau}}^p \tag{3.12}$$

Thus, Equation (3.6) becomes

$$\lambda\left[\frac{\partial \tau_{ij}}{\partial t} + v_k \frac{\partial \tau_{ij}}{\partial x_k} - \frac{\partial v_j}{\partial x_k}\tau_{ki} - \frac{\partial v_i}{\partial x_k}\tau_{kj}\right] + \tau_{ij} = \mu_p\left[\frac{\partial v_i}{\partial x_j} + \frac{\partial v_j}{\partial x_i}\right] \tag{3.13}$$

3.1.2. Boundary and Interface Conditions

At the bottom wall, $z = -h^{(1)}$, the no-slip condition is

$$v_x = 0 \tag{3.14}$$

the no-flow through the wall is

$$v_z = 0 \tag{3.15}$$

and the applied voltage is

$$V^{(1)} = V_b \tag{3.16}$$

At the top wall, $z = h^{(2)}$, due to the air has no velocity, there is only the applied voltage condition, which is

$$V^{(2)} = 0 \tag{3.17}$$

At the interface, z = Z (x, t), the normal component of the velocity is equal to u which is the velocity of the interface,

$$\underline{v}.\underline{n} = u \tag{3.18}$$

and the electric field is continuous,

$$\left[\underline{E}^{(j)}.\underline{t}\right]_1^2 = 0 \tag{3.19}$$

where $\underline{E}$ represents the electric field. $[\ ]_1^2$ denotes the jump in the variables at the interface. $\underline{n}$, $\underline{t}$, and u represent the unit normal vector, unit tangent vector, and the normal speed of the interface, respectively, which are expressed as below,

$$\underline{n} = \frac{\underline{e}_z - \frac{\partial Z}{\partial x}\underline{e}_x}{\sqrt{1 + \left(\frac{\partial Z}{\partial x}\right)^2}} \tag{3.20}$$

$$\underline{t} = \frac{\underline{e}_x + \frac{\partial Z}{\partial x}\underline{e}_z}{\sqrt{1 + \left(\frac{\partial Z}{\partial x}\right)^2}} \tag{3.21}$$

$$u = \frac{\frac{\partial Z}{\partial t}}{\sqrt{1 + \left(\frac{\partial Z}{\partial x}\right)^2}} \tag{3.22}$$

where $\underline{e}_x$ and $\underline{e}_z$ are the unit base vectors.

The surface charge density is defined by the Gauss' law for the electric field as

$$q = \left[\varepsilon_0 \varepsilon \underline{E}^{(j)}.\underline{n}\right]_1^2 \tag{3.23}$$

The charge distribution at the interface is expressed as

$$q_t - \underline{u}.\nabla_s q + \nabla_s.\left(q\underline{u}_s\right) + q2H\underline{u}.\underline{n} = -\left[\sigma^{(j)}\underline{E}^{(j)}.\underline{n}\right]_1^2 \tag{3.24}$$

where q_t, and $\underline{u_s}$ represent the time derivative of the charge density, and the surface velocity, respectively. ∇_s is the surface gradient (Castellanos and González, 1998), and 2H is twice the surface mean curvature (Johns and Narayanan, 2002) which are defined as follows:

$$\nabla_s = \nabla - \underline{n}(\underline{n}.\nabla) \tag{3.25}$$

$$2H = \frac{\frac{\partial^2 Z}{\partial x^2}}{\left(\sqrt{1+\left(\frac{\partial Z}{\partial x}\right)^2}\right)^{3/2}} \tag{3.26}$$

The stress balance at the interface is given by

$$\left[\underline{\underline{T}}^{(j)}\right]_1^2 . \underline{n} + \gamma 2H\underline{n} = 0 \tag{3.27}$$

where $\underline{\underline{T}}$ is the total stress tensor, γ is the interfacial tensor. Equation (3.27) yields the normal stress balance (NSB) when dotted with the normal vector, and the tangential stress balance (TSB) when dotted with the tangent vector as:

$$\left[\underline{\underline{T}}^{(j)}\right]_1^2 . \underline{n}.\underline{n} + \gamma 2H = 0 \tag{3.28}$$

$$\left[\underline{\underline{T}}^{(j)}\right]_1^2 . \underline{n}.\underline{t} = 0 \tag{3.29}$$

The total stress tensor $\underline{\underline{T}}$ consists of a fluid component $\underline{\underline{T}}^F$, and an electrical component $\underline{\underline{T}}^{E^{(j)}}$, i.e.,

$$\underline{\underline{T}}^{(j)} = \underline{\underline{T}}^F + \underline{\underline{T}}^{E^{(j)}} \tag{3.30}$$

The superscript for the fluid component is omitted as air is assumed to be passive. $\underline{\underline{T}}^{F}$ and $\underline{\underline{T}}^{E^{(j)}}$ are defined as

$$\underline{\underline{T}}^{F} = -p\underline{\underline{I}} + \underline{\underline{\tau}} \tag{3.31}$$

$$\underline{\underline{T}}^{E^{(j)}} = \varepsilon_0 \varepsilon \left(\underline{E}^{(j)} \underline{E}^{(j)} - \frac{1}{2} \left| \underline{E}^{(j)} \right|^2 \underline{\underline{I}} \right) \tag{3.32}$$

where $\underline{\underline{I}}$ is the identity tensor.

The definition of the electric field in the Cartesian coordinates is

$$\underline{E}^{(j)} = -\nabla V^{(j)} = -\left(\frac{\partial V^{(j)}}{\partial x} \underline{e}_x + \frac{\partial V^{(j)}}{\partial z} \underline{e}_z\right) \tag{3.33}$$

Thus, Equation (3.27) can be written as

$$\begin{aligned} &\left\{ \varepsilon_0 \varepsilon^{(2)} \left(\underline{E}^{(2)} \underline{E}^{(2)} - \frac{1}{2} \left| \underline{E}^{(2)} \right|^2 \underline{I} \right) \right\} . \underline{n} \\ &- \left\{ -p\underline{\underline{I}} + \underline{\underline{\tau}} + \varepsilon_0 \varepsilon^{(1)} \left(\underline{E}^{(1)} \underline{E}^{(1)} - \frac{1}{2} \left| \underline{E}^{(1)} \right|^2 \underline{\underline{I}} \right) \right\} . \underline{n} = -\gamma 2H \underline{n} \end{aligned} \tag{3.34}$$

The NSB, Equation (3.28), and the TSB, Equation (3.29) are found as

$$\begin{aligned} &\left\{ \varepsilon_0 \varepsilon^{(2)} \left(\underline{E}^{(2)} \underline{E}^{(2)} - \frac{1}{2} \left| \underline{E}^{(2)} \right|^2 \underline{\underline{I}} \right) \right\} . \underline{n} . \underline{n} \\ &- \left\{ -p\underline{\underline{I}} + \underline{\underline{\tau}} + \varepsilon_0 \varepsilon^{(1)} \left(\underline{E}^{(1)} \underline{E}^{(1)} - \frac{1}{2} \left| \underline{E}^{(1)} \right|^2 \underline{\underline{I}} \right) \right\} . \underline{n} . \underline{n} + \gamma 2H = 0 \end{aligned} \tag{3.35}$$

$$\left(\underline{\underline{\tau}} . \underline{n} . \underline{t} \right) + \left(\varepsilon_0 \varepsilon^{(1)} \underline{E}^{(1)} \underline{E}^{(1)} . \underline{n} . \underline{t} \right) = \left(\varepsilon_0 \varepsilon^{(2)} \underline{E}^{(2)} \underline{E}^{(2)} . \underline{n} . \underline{t} \right) \tag{3.36}$$

respectively.

3.1.3. Scaling

All system variables are scaled with respect to the first fluid's, i.e. UCM fluid's, parameters. The variables are written in dimensionless form as

$$x = \overline{x}\tilde{x} \tag{3.37}$$

where $\tilde{x}$ is dimensionless variable, and $\overline{x}$ is the dimension of the variable, i.e., the scale factor. The scale factors for the variables are given as

$$\begin{gathered}\overline{v} = \frac{\gamma}{\mu_p};\ \overline{x} = \overline{z} = \overline{L} = h^{(1)};\quad \overline{t} = \frac{\overline{L}}{\overline{v}} = \frac{h^{(1)}\mu_p}{\gamma};\ \overline{p} = \overline{\tau} = \frac{\mu_p \overline{v}}{h^{(1)}} = \frac{\gamma}{h^{(1)}};\\ \overline{V} = V_b;\ \overline{q} = \frac{\varepsilon_0 V_b}{h^{(1)}};\quad \overline{E} = \frac{V_b}{h^{(1)}};\ \overline{D} = \frac{\overline{v}}{h^{(1)}} = \frac{\gamma}{\mu_p h^{(1)}};\ \overline{\nabla} = \frac{1}{h^{(1)}}\end{gathered} \tag{3.38}$$

3.1.3.1. Governing Equations in Dimensionless Form. The equation of motion for the first fluid (UCM) in dimensionless form is

$$Re\left[\frac{\partial \tilde{\underline{v}}}{\partial \tilde{t}} + \tilde{\underline{v}}.\tilde{\nabla}\tilde{\underline{v}}\right] = -\tilde{\nabla}\mathrm{p} + \tilde{\nabla}.\tilde{\underline{\underline{\tau}}} \tag{3.39}$$

Here, Re expresses the Reynolds number, and is defined as

$$Re = \frac{\rho \overline{v}\overline{L}}{\mu_p} = \frac{\rho\gamma h^{(1)}}{{\mu_p}^2} \tag{3.40}$$

Equation (3.13), the UCM model, is scaled as

$$\begin{gathered}\lambda\frac{\gamma^2}{{h^{(1)}}^2\mu_p}\left[\frac{\partial \tilde{\tau}_{ij}}{\partial \tilde{t}} + \tilde{v}_k\frac{\partial \tilde{\tau}_{ij}}{\partial \tilde{x}_k} - \frac{\partial \tilde{v}_j}{\partial \tilde{x}_k}\tilde{\tau}_{ki} - \frac{\partial \tilde{v}_i}{\partial \tilde{x}_k}\tilde{\tau}_{kj}\right]\\ + \frac{\gamma}{h^{(1)}}\tilde{\tau}_{ij} = \frac{\gamma}{h^{(1)}}\left[\frac{\partial \tilde{v}_i}{\partial \tilde{x}_j} + \frac{\partial \tilde{v}_j}{\partial \tilde{x}_i}\right]\end{gathered} \tag{3.41}$$

and dividing by $\frac{\gamma}{h^{(1)}}$,

$$\tilde{\tau}_{ij} + We\left[\frac{\partial\tilde{\tau}_{ij}}{\partial\tilde{t}} + \tilde{v}_k\frac{\partial\tilde{\tau}_{ij}}{\partial\tilde{x}_k} - \frac{\partial\tilde{v}_j}{\partial\tilde{x}_k}\tilde{\tau}_{ki} - \frac{\partial\tilde{v}_i}{\partial\tilde{x}_k}\tilde{\tau}_{kj}\right] = \left[\frac{\partial\tilde{v}_i}{\partial\tilde{x}_j} + \frac{\partial\tilde{v}_j}{\partial\tilde{x}_i}\right] \tag{3.42}$$

is obtained. Here, We is the Weissenberg number that is the ratio of relaxation time of the fluid to time scale, and its definition is

$$We = \frac{\lambda}{\bar{t}} = \frac{\lambda\,\gamma}{h^{(1)}\mu_p} \tag{3.43}$$

The expansion of Equation (3.42) is obtained as follows:

- For i=x, and j=x, $\tilde{\tau}_{xx}$ is expanded as

$$\tilde{\tau}_{xx} + We\left[\frac{\partial\tilde{\tau}_{xx}}{\partial\tilde{t}} + \tilde{v}_x\frac{\partial\tilde{\tau}_{xx}}{\partial\tilde{x}} + \tilde{v}_z\frac{\partial\tilde{\tau}_{xx}}{\partial\tilde{z}} - 2\frac{\partial\tilde{v}_x}{\partial\tilde{x}}\tilde{\tau}_{xx} - 2\frac{\partial\tilde{v}_x}{\partial\tilde{z}}\tilde{\tau}_{zx}\right] = 2\frac{\partial\tilde{v}_x}{\partial\tilde{x}} \tag{3.44}$$

- For i=x, and j=x, $\tilde{\tau}_{xz}$ is

$$\tilde{\tau}_{xz} + We\left[\frac{\partial\tilde{\tau}_{xz}}{\partial\tilde{t}} + \tilde{v}_x\frac{\partial\tilde{\tau}_{xz}}{\partial\tilde{z}} + \tilde{v}_z\frac{\partial\tilde{\tau}_{xz}}{\partial\tilde{z}} - \frac{\partial\tilde{v}_z}{\partial\tilde{x}}\tilde{\tau}_{xx} - \frac{\partial\tilde{v}_x}{\partial\tilde{z}}\tilde{\tau}_{zz}\right] = \frac{\partial\tilde{v}_x}{\partial\tilde{z}} + \frac{\partial\tilde{v}_z}{\partial\tilde{x}} \tag{3.45}$$

- For i=z, and i=z, $\tilde{\tau}_{zz}$ is

$$\tilde{\tau}_{zz} + We\left[\frac{\partial\tilde{\tau}_{zz}}{\partial\tilde{t}} + \tilde{v}_x\frac{\partial\tilde{\tau}_{zz}}{\partial\tilde{x}} + \tilde{v}_z\frac{\partial\tilde{\tau}_{zz}}{\partial\tilde{z}} - 2\frac{\partial\tilde{v}_z}{\partial\tilde{x}}\tilde{\tau}_{xz} - 2\frac{\partial\tilde{v}_z}{\partial\tilde{z}}\tilde{\tau}_{zz}\right] = 2\frac{\partial\tilde{v}_z}{\partial\tilde{z}} \tag{3.46}$$

The continuity equation for the first fluid, and the Laplace equation for both fluids in dimensionless form are

$$\tilde{\nabla}.\underline{\tilde{v}} = 0 \tag{3.47}$$

$$\tilde{\nabla}^2\tilde{V}^{(j)} = 0 \tag{3.48}$$

respectively.

3.1.3.2. Boundary and Interface Conditions in Dimensionless Form. At the bottom wall, $\tilde{z} = -1$,

$$\tilde{v}_x = 0 \tag{3.49}$$

$$\tilde{v}_z = 0 \tag{3.50}$$

$$\tilde{V}^{(1)} = 1 \tag{3.51}$$

at the top wall, $\tilde{z} = Hr$,

$$\tilde{V}^{(2)} = 0 \tag{3.52}$$

Here, Hr is the thickness ratio of the fluids which is

$$Hr = \frac{h^{(2)}}{h^{(1)}} \tag{3.53}$$

At the interface, $\tilde{z} = \tilde{Z}(\tilde{x}, \tilde{t})$, Equations (3.18)-(3.19), and the Equation (3.23) in dimensionless form are found as

$$\underline{\tilde{v}}.\underline{n} = \tilde{u} \tag{3.54}$$

$$\left[\underline{\tilde{E}}^{(j)}.\underline{t}\right]_1^2 = 0 \tag{3.55}$$

$$\tilde{q} = \left[\varepsilon^{(j)}\underline{\tilde{E}}^{(j)}.\underline{n}\right]_1^2 \tag{3.56}$$

respectively. The charge balance at the interface, Equation (3.24), in dimensionless form is

$$\frac{\varepsilon_0 V_b \gamma}{h^{(1)^2}\mu_p}\tilde{q}_t - \frac{\varepsilon_0 V_b \gamma}{h^{(1)^2}\mu_p}\underline{\tilde{u}}.\tilde{\nabla}_s\tilde{q} + \frac{\varepsilon_0 V_b \gamma}{h^{(1)^2}\mu_p}\nabla_s.\left(\tilde{q}\underline{\tilde{u}}_s\right) + \frac{\varepsilon_0 V_b \gamma}{h^{(1)^2}\mu_p}\tilde{q}2\tilde{H}\underline{\tilde{u}}.\underline{n} = -\frac{V_b}{h^{(1)}}\left[\sigma^{(j)}\underline{\tilde{E}}^{(j)}.\underline{n}\right]_1^2 \tag{3.57}$$

and is simplified as

$$\tilde{q}_t - \underline{\tilde{u}}.\tilde{\nabla}_s\tilde{q} + \tilde{\nabla}_s.\left(\tilde{q}\underline{\tilde{u}}_s\right) + \tilde{q}2\tilde{H}\underline{\tilde{u}}.\underline{n} = S(\underline{\tilde{E}}^{(1)}.\underline{n} - \sigma_r\underline{\tilde{E}}^{(2)}.\underline{n}) \tag{3.58}$$

where S is the ratio of fluid time scale to electric time scale, and σ_r is the ratio of electrical conductivities of the fluids, which are

$$S = \frac{t_F}{t_E} = \frac{h^{(1)}\mu_p\sigma^{(1)}}{\gamma\varepsilon_0} \tag{3.59}$$

$$\sigma_r = \frac{\sigma^{(2)}}{\sigma^{(1)}} \tag{3.60}$$

The tangential stress balance (TSB), Equation (3.36), in dimensionless form is

$$\frac{\gamma}{h^{(1)}}\left(\underline{\tilde{\tau}}.\underline{n}.\underline{t}\right) + \varepsilon_0\varepsilon^{(1)}\frac{V_b^2}{h^{(1)^2}}\left(\underline{\tilde{E}}^{(1)}\underline{\tilde{E}}^{(1)}.\underline{n}.\underline{t}\right) = \varepsilon_0\varepsilon^{(2)}\frac{V_b^2}{h^{(1)^2}}\left(\underline{\tilde{E}}^{(2)}\underline{\tilde{E}}^{(2)}.\underline{n}.\underline{t}\right) \tag{3.61}$$

and is simplified as

$$\left(\underline{\tilde{\tau}}.\underline{n}.\underline{t}\right) + \varepsilon^{(1)}E_b\left(\underline{\tilde{E}}^{(1)}\underline{\tilde{E}}^{(1)}.\underline{n}.\underline{t}\right) = \varepsilon^{(2)}E_b\left(\underline{\tilde{E}}^{(2)}\underline{\tilde{E}}^{(2)}.\underline{n}.\underline{t}\right) \tag{3.62}$$

where E_b is the dimensionless electric number that is defined as

$$E_b = \varepsilon_0\frac{V_b^2}{h^{(1)}\gamma} \tag{3.63}$$

The normal stress balance (NSB), Equation (3.35), in dimensionless form is

$$\begin{aligned}&\left\{\varepsilon_0\varepsilon^{(2)}\frac{V_b^2}{h^{(1)^2}}\left(\underline{\tilde{E}}^{(2)}\underline{\tilde{E}}^{(2)}-\frac{1}{2}\left|\underline{\tilde{E}}^{(2)}\right|^2\underline{\underline{I}}\right)\right\}.\underline{n}.\underline{n}\\-&\left\{-\frac{\gamma}{h^{(1)}}\tilde{p}\underline{\underline{I}}+\frac{\gamma}{h^{(1)}}\underline{\underline{\tilde{\tau}}}+\varepsilon_0\varepsilon^{(1)}\frac{V_b^2}{h^{(1)^2}}\left(\underline{\tilde{E}}^{(1)}\underline{\tilde{E}}^{(1)}-\frac{1}{2}\left|\underline{\tilde{E}}^{(1)}\right|^2\underline{\underline{I}}\right)\right\}.\underline{n}.\underline{n}\\&+\gamma 2\tilde{H}=0\end{aligned}\tag{3.64}$$

which becomes

$$\begin{aligned}&\left\{\varepsilon^{(2)}E_b\left(\underline{\tilde{E}}^{(2)}\underline{\tilde{E}}^{(2)}-\frac{1}{2}\left|\underline{\tilde{E}}^{(2)}\right|^2\underline{\underline{I}}\right)\right\}.\underline{n}.\underline{n}\\-&\left\{-\tilde{p}\underline{\underline{I}}+\underline{\underline{\tilde{\tau}}}+\varepsilon^{(1)}E_b\left(\underline{\tilde{E}}^{(1)}\underline{\tilde{E}}^{(1)}-\frac{1}{2}\left|\underline{\tilde{E}}^{(1)}\right|^2\underline{\underline{I}}\right)\right\}.\underline{n}.\underline{n}+2\tilde{H}=0\end{aligned}\tag{3.65}$$

The (˜) symbol used for nondimensionalization, is removed for simplicity, since all system variables are converted to dimensionless form. The summary of the scaled governing equations, boundary and interface conditions are given in Table 3.1 and Table 3.2. The dimensionless parameters are listed in Table 3.3.

Table 3.1. Summary of the scaled governing equations.

For the first fluid at $-1 < z < Z(\mathrm{x,t})$	$Re\left[\frac{\partial v_x}{\partial t} + v_x\frac{\partial v_x}{\partial x} + v_z\frac{\partial v_x}{\partial z}\right] = -\frac{\partial p}{\partial x} + \left(\frac{\partial \tau_{xx}}{\partial x} + \frac{\partial \tau_{xz}}{\partial z}\right)$
	$Re\left[\frac{\partial v_z}{\partial t} + v_x\frac{\partial v_z}{\partial x} + v_z\frac{\partial v_z}{\partial z}\right] = -\frac{\partial p}{\partial z} + \left(\frac{\partial \tau_{xz}}{\partial x} + \frac{\partial \tau_{zz}}{\partial z}\right)$
	$\frac{\partial v_x}{\partial x} + \frac{\partial v_z}{\partial z} = 0$
	$\frac{\partial^2 V^{(1)}}{\partial x^2} + \frac{\partial^2 V^{(1)}}{\partial z^2} = 0$
	$\tau_{xx} + We\left[\frac{\partial \tau_{xx}}{\partial t} + v_x\frac{\partial \tau_{xx}}{\partial x} + v_z\frac{\partial \tau_{xx}}{\partial z} - 2\frac{\partial v_x}{\partial x}\tau_{xx} - 2\frac{\partial v_x}{\partial z}\tau_{zx}\right] = 2\frac{\partial v_x}{\partial x}$
	$\tau_{xz} + We\left[\frac{\partial \tau_{xz}}{\partial t} + v_x\frac{\partial \tau_{xz}}{\partial z} + v_z\frac{\partial \tau_{xz}}{\partial z} - \frac{\partial v_z}{\partial x}\tau_{xx} - \frac{\partial v_x}{\partial z}\tau_{zz}\right] = \frac{\partial v_x}{\partial z} + \frac{\partial v_z}{\partial x}$
	$\tau_{zz} + We\left[\frac{\partial \tau_{zz}}{\partial t} + v_x\frac{\partial \tau_{zz}}{\partial x} + v_z\frac{\partial \tau_{zz}}{\partial z} - 2\frac{\partial v_z}{\partial x}\tau_{xz} - 2\frac{\partial v_z}{\partial z}\tau_{zz}\right] = 2\frac{\partial v_z}{\partial z}$
For air at $\mathrm{Z(x,t)} < z < Hr$	$\frac{\partial^2 V^{(2)}}{\partial x^2} + \frac{\partial^2 V^{(2)}}{\partial z^2} = 0$

Table 3.2. Summary of the scaled boundary and interface conditions.

At the bottom wall, z = -1	$v_x = 0$
	$v_z = 0$
	$V^{(1)} = 1$
At the top wall, z = Hr	$V^{(2)} = 0$
At the interface, z = Z (x , t)	$\underline{v}.\underline{n} = u$
	$\left[\underline{E}^{(j)}.\underline{t}\right]_1^2 = 0$
	$q = \left[\varepsilon^{(j)}\underline{E}^{(j)}.\underline{n}\right]_1^2$
	$q_t - \underline{u}.\nabla_s q + \nabla_s.\left(q\underline{u}_s\right) + q2H\underline{u}.\underline{n} = -S\left[\sigma_r\underline{E}^{(j)}.\underline{n}\right]_1^2$
	$\left\{\varepsilon^{(2)}E_b\left(\underline{E}^{(2)}\underline{E}^{(2)} - \frac{1}{2}\left\|\underline{E}^{(2)}\right\|^2\underline{\underline{I}}\right)\right\}.\underline{n}.\underline{n}$ $-\left\{-p\underline{\underline{I}} + \underline{\underline{\tau}} + \varepsilon^{(1)}E_b\left(\underline{E}^{(1)}\underline{E}^{(1)} - \frac{1}{2}\left\|\underline{E}^{(1)}\right\|^2\underline{\underline{I}}\right)\right\}.\underline{n}.\underline{n} + 2H = 0$
	$\left(\underline{\underline{\tau}}.\underline{n}.\underline{t}\right) + \varepsilon^{(1)}E_b\left(\underline{E}^{(1)}\underline{E}^{(1)}.\underline{n}.\underline{t}\right) = \varepsilon^{(2)}E_b\left(\underline{E}^{(2)}\underline{E}^{(2)}.\underline{n}.\underline{t}\right)$

Table 3.3. List of the dimensionless parameters.

Dimensionless parameter	Definition
Reynolds number	$Re = \frac{\rho \gamma h^{(1)}}{{\mu_p}^2}$
Weissenberg number	$We = \frac{\lambda \gamma}{h^{(1)} \mu_p}$
Thickness ratio	$Hr = \frac{h^{(2)}}{h^{(1)}}$
Conductivity ratio	$\sigma_r = \frac{\sigma^{(2)}}{\sigma^{(1)}}$
Electric number	$E_b = \varepsilon_0 \frac{V_b^2}{h^{(1)} \gamma}$
Electric time scale	$S = \frac{h^{(1)} \mu_p \sigma^{(1)}}{\gamma \varepsilon_0}$

3.1.4. Linear Stability Analysis

Nonlinear equations introduced in the previous sections are linearized around a base state, and the stability of the interface between the two fluids is analyzed. The linearization is carried out as follows (Johns and Narayanan, 2002)

$$n = n_0 + \epsilon \left(n_1 + z_1 \frac{\partial n_0}{\partial z_0} \right) + O(\epsilon^2) \tag{3.66}$$

Thereby, the response of the system to an infinitesimally small perturbation (ϵ) is analyzed. Here, z_1 represents the mapping from the reference domain to the current domain, which becomes Z_1 at the interface. The indices 0 and 1 denote the base, and the perturbed states, respectively. The time and the x-coordinate dependences of the variables are separated by the normal mode expansion as

$$n_1 = \hat{n}_1(z_0) e^{\omega t_0} e^{ikx_0} \tag{3.67}$$

where, 'k' is the wave number, and 'ω' is the growth/decay rate of the given disturbance (Johns and Narayanan, 2002). The value of 'ω' determines whether or not the system is stable to a given infinitesimal disturbance. The system is unstable when the real part of 'ω' is positive and the disturbance grows in time. When the real part of the 'ω' is negative, the system is stable and the disturbance disappears in time.

3.1.4.1. Base State (ϵ^0). The base state is assumed to be stationary, so

$$\underline{v}_0 = \underline{0} \tag{3.68}$$

The Laplace equation for both fluids, at the base state is

$$\nabla_0{}^2 V_0{}^{(j)} = 0 \tag{3.69}$$

$$\underbrace{\frac{d^2 V_0{}^{(j)}}{dx_0{}^2}}_{0} + \frac{d^2 V_0{}^{(j)}}{dz_0{}^2} = 0 \tag{3.70}$$

and $V_0{}^{(j)}$ is found as

$$V_0{}^{(j)} = D_0{}^{(j)} z_0 + F_0{}^{(j)} \tag{3.71}$$

By applying the boundary and interface conditions, the voltage potentials for the base state are found as

$$V_0{}^{(1)} = -\frac{\sigma_r}{Hr + \sigma_r} z_0 + \frac{Hr}{Hr + \sigma_r} \tag{3.72}$$

$$V_0^{(2)} = -\frac{1}{Hr + \sigma_r} z_0 + \frac{Hr}{Hr + \sigma_r} \tag{3.73}$$

Then, the electric field equation for both fluids, at the base state, are obtained as

$$\underline{E_0}^{(j)} = -\left(\frac{dV_0{}^{(j)}}{dx_0}\underline{e}_{x0} + \frac{dV_0{}^{(j)}}{dz_0}\underline{e}_{z0}\right) \tag{3.74}$$

Equation (3.91) is then substituted into Gauss' law at the base state which is

$$q_0 = \left[\varepsilon^{(j)}\underline{E_0}^{(j)}.\underline{n}_0\right]_1^2 \tag{3.75}$$

and finally the surface charge density at the base state is found as

$$q_0 = \frac{\varepsilon^{(2)} - \varepsilon^{(1)}\sigma_r}{Hr + \sigma_r} \tag{3.76}$$

3.1.4.2. Perturbed State (ϵ^1). The terms with ϵ^1 coefficient in the governing equations and the boundary and the interface conditions are derived to investigate the linear stability of the system.

The x- and z-components of the equation of motion, and the continuity equation for the first fluid, and the Laplace equation for both fluids at the perturbed state are found as

$$Re\left[\frac{\partial v_{x1}}{\partial t_0} + v_{x0}\frac{\partial v_{x1}}{\partial x_0} + v_{z1}\frac{\partial v_{x0}}{\partial z_0}\right] = -\frac{\partial p_1}{\partial x_0} + \left[\frac{\partial \tau_{xx1}}{\partial x_0} + \frac{\partial \tau_{zx1}}{\partial z_0}\right] \tag{3.77}$$

$$Re\left[\frac{\partial v_{z1}}{\partial t_0} + v_{x0}\frac{\partial v_{z1}}{\partial x_0}\right] = -\frac{\partial p_1}{\partial z_0} + \left[\frac{\partial \tau_{xz1}}{\partial x_0} + \frac{\partial \tau_{zz1}}{\partial z_0}\right] \tag{3.78}$$

$$\frac{\partial v_{x1}}{\partial x_0} + \frac{\partial v_{z1}}{\partial z_0} = 0 \tag{3.79}$$

and

$$\frac{\partial^2 V_1{}^{(j)}}{\partial {x_0}^2} + \frac{\partial^2 V_1{}^{(j)}}{\partial {z_0}^2} = 0 \tag{3.80}$$

respectively. The stress tensor components at the perturbed state are

$$\tau_{xx1} + We\left[\frac{\partial \tau_{xx1}}{\partial t_0} + v_{x0}\frac{\partial \tau_{xx1}}{\partial x_0} + v_{z1}\frac{\partial \tau_{xx0}}{\partial z_0} - 2\frac{\partial v_{x1}}{\partial x_0}\tau_{xx0} - 2\frac{\partial v_{x0}}{\partial z_0}\tau_{zx1} - 2\frac{\partial v_{x1}}{\partial z_0}\tau_{zx0}\right] = 2\frac{\partial v_{x1}}{\partial x_0} \tag{3.81}$$

$$\tau_{xx1} + We\left[\frac{\partial \tau_{xx1}}{\partial t_0} + v_{x0}\frac{\partial \tau_{xx1}}{\partial x_0} + v_{z1}\frac{\partial \tau_{xx0}}{\partial z_0} - 2\frac{\partial v_{x1}}{\partial x_0}\tau_{xx0} - 2\frac{\partial v_{x0}}{\partial z_0}\tau_{zx1} - 2\frac{\partial v_{x1}}{\partial z_0}\tau_{zx0}\right] = 2\frac{\partial v_{x1}}{\partial x_0} \tag{3.82}$$

$$\tau_{zz1} + We\left[\frac{\partial \tau_{zz1}}{\partial t_0} + v_{x0}\frac{\partial \tau_{zz1}}{\partial x_0} - 2\frac{\partial v_{z1}}{\partial x_0}\tau_{xz0}\right] = 2\frac{\partial v_{z1}}{\partial z_0} \tag{3.83}$$

The detailed derivations of the boundary and the interface conditions at the perturbed state and $\underline{n}_1$, $\underline{n}_0$, $\underline{t}_1$, $\underline{t}_0$ and u are given in Appendix A.

At the bottom wall, $z_0 = -1$, the perturbed boundary conditions are

$$v_{x1} = 0 \tag{3.84}$$

$$v_{z1} = 0 \tag{3.85}$$

$$V_1{}^{(1)} = 0 \tag{3.86}$$

and at the top wall, $z_0 = Hr$,

$$V_1{}^{(2)} = 0 \tag{3.87}$$

At the interface, $z_0 = 0$, Equations (3.54), (3.55), and (3.56) are expanded in Taylor series to find the perturbed interface conditions, which are

$$v_{z1} - v_{x0}\frac{\partial Z_1}{\partial x_0} = \frac{\partial Z_1}{\partial t_0} \tag{3.88}$$

$$\left[\frac{\partial V_1{}^{(j)}}{\partial x_0} + \frac{\partial Z_1}{\partial x_0}\frac{\partial V_0{}^{(j)}}{\partial z_0}\right]_1^2 = 0 \tag{3.89}$$

$$q_1 = \left[\varepsilon^{(j)}\left(-\frac{\partial V_1^{(j)}}{\partial z_0}\right)\right]_1^2 \tag{3.90}$$

$$\frac{\partial q_1}{\partial t_0} - v_{x0}\frac{\partial q_1}{\partial x_0} + q_0\frac{\partial v_{x1}}{\partial x_0} = S\left(\sigma_r\frac{\partial V_1^{(2)}}{\partial z_0} - \frac{\partial V_1{}^{(1)}}{\partial z_0}\right) \tag{3.91}$$

respectively.

Finally, the NSB, Equation (3.62), and the TSB, Equation (3.65), are written at the perturbed state as

$$-p_1 + \tau_{zz1} - 2\frac{\partial Z_1}{\partial x_0}\tau_{xz0} - \left[\varepsilon^{(j)}E_b\left(\frac{\partial V_0{}^{(j)}}{\partial z_0}\frac{\partial V_1{}^{(j)}}{\partial z_0}\right)\right]_1^2 = \frac{\partial^2 Z_1}{\partial {x_0}^2} \tag{3.92}$$

and

$$\tau_{xz1} + Z_1\frac{\partial \tau_{xz0}}{\partial z_0} - \frac{\partial Z_1}{\partial x_0}\tau_{xx0} - \left[\varepsilon^{(j)}E_b\left(\frac{\partial V_0{}^{(j)}}{\partial z_0}\frac{\partial V_1{}^{(j)}}{\partial x_0} + \frac{\partial Z_1}{\partial x_0}\left(\frac{\partial V_0{}^{(j)}}{\partial z_0}\right)^2\right)\right]_1^2 = 0 \tag{3.93}$$

respectively. The perturbed governing equations, and the perturbed boundary and interface conditions are derived in their general form including the base state velocities even though they will eventually be assumed to be zero.

The perturbed governing equations, and the perturbed boundary and interface conditions are given in Table 3.4 and Table 3.5, respectively.

By applying the normal mode expansion, as in Equation (3.67), to all parameters in Table 3.4 and Table 3.5, the governing equations are obtained as in Table 3.6, and the boundary and interface conditions are obtained as in Table 3.7.

Table 3.4. Summary of the perturbed equations for a non-Newtonian fluid and air system under the influence of a normal electric field.

For the first fluid at $-1 < z_0 < 0$	$Re\left[\frac{\partial v_{x1}}{\partial t_0} + v_{x0}\frac{\partial v_{x1}}{\partial x_0} + v_{z1}\frac{dv_{x0}}{dz_0}\right] = -\frac{\partial p_1}{\partial x_0} + [\frac{\partial \tau_{xx1}}{\partial x_0} + \frac{\partial \tau_{zx1}}{\partial z_0}]$
	$Re\left[\frac{\partial v_{z1}}{\partial t_0} + v_{x0}\frac{\partial v_{z1}}{\partial x_0}\right] = -\frac{\partial p_1}{\partial z_0} + [\frac{\partial \tau_{xz1}}{\partial x_0} + \frac{\partial \tau_{zz1}}{\partial z_0}]$
	$\frac{\partial v_{x1}}{\partial x_0} + \frac{\partial v_{z1}}{\partial z_0} = 0$
	$\frac{\partial^2 V_1^{(1)}}{\partial {x_0}^2} + \frac{\partial^2 V_1^{(1)}}{\partial {z_0}^2} = 0$
	$\tau_{xx1} + We\left[\frac{\partial \tau_{xx1}}{\partial t_0} + v_{x0}\frac{\partial \tau_{xx1}}{\partial x_0} + v_{z1}\frac{\partial \tau_{xx0}}{\partial z_0} - 2\frac{\partial v_{x1}}{\partial x_0}\tau_{xx0} - 2\frac{dv_{x0}}{dz_0}\tau_{zx1} - 2\frac{\partial v_{x1}}{\partial z_0}\tau_{zx0}\right] = 2\frac{\partial v_{x1}}{\partial x_0}$
	$\tau_{xz1} + We\left[\frac{\partial \tau_{xz1}}{\partial t_0} + v_{x0}\frac{\partial \tau_{xz1}}{\partial z_0} + v_{z1}\frac{\partial \tau_{xz0}}{\partial z_0} - \frac{\partial v_{z1}}{\partial x_0}\tau_{xx0} - \frac{dv_{x0}}{dz_0}\tau_{zz1}\right] = \frac{\partial v_{x1}}{\partial z_0} + \frac{\partial v_{z1}}{\partial x_0}$
	$\tau_{zz1} + We\left[\frac{\partial \tau_{zz1}}{\partial t_0} + v_{x0}\frac{\partial \tau_{zz1}}{\partial x_0} - 2\frac{\partial v_{z1}}{\partial x_0}\tau_{xz0}\right] = 2\frac{\partial v_{z1}}{\partial z_0}$
For the second fluid at $0 < z_0 < Hr$	$\frac{\partial^2 V_1^{(2)}}{\partial {x_0}^2} + \frac{\partial^2 V_1^{(2)}}{\partial {z_0}^2} = 0$

Table 3.5. Summary of the boundary and interface conditions for a non-Newtonian fluid and air system under the influence of a normal electric field.

At the bottom wall, $z_0 = -1$	$v_{x1} = 0$
	$v_{z1} = 0$
	$V_1^{(1)} = 0$
At the top wall, $z_0 = Hr$	$V_1^{(2)} = 0$
At the interface, $z_0 = 0$	$v_{z1} - v_{x0}\frac{\partial Z_1}{\partial x_0} = \frac{\partial Z_1}{\partial t_0}$
	$\left[\frac{\partial V_1^{(j)}}{\partial x_0} + \frac{\partial Z_1}{\partial x_0}\frac{\partial V_0^{(j)}}{\partial z_0}\right]_1^2 = 0$
	$q_1 = \left[\varepsilon^{(j)}\left(-\frac{\partial V_1^{(j)}}{\partial z_0}\right)\right]_1^2$
	$\frac{\partial q_1}{\partial t_0} - v_{x0}\frac{\partial q_1}{\partial x_0} + q_0\frac{\partial v_{x1}}{\partial x_0} = S\left(\sigma_r\frac{\partial V_1^{(2)}}{\partial z_0} - \frac{\partial V_1^{(1)}}{\partial z_0}\right)$
	$-p_1 + \tau_{zz1} - 2\frac{\partial Z_1}{\partial x_0}\tau_{xz0} - \left[\varepsilon^{(j)}E_b\left(\frac{\partial V_0^{(j)}}{\partial z_0}\frac{\partial V_1^{(j)}}{\partial z_0}\right)\right]_1^2 = \frac{\partial^2 Z_1}{\partial {x_0}^2}$
	$\tau_{xz1} + Z_1\frac{\partial \tau_{xz0}}{\partial z_0} - \frac{\partial Z_1}{\partial x_0}\tau_{xx0} - \left[\varepsilon^{(j)}E_b\left(\frac{\partial V_0^{(j)}}{\partial z_0}\frac{\partial V_1^{(j)}}{\partial x_0} + \frac{\partial Z_1}{\partial x_0}\left(\frac{\partial V_0^{(j)}}{\partial z_0}\right)^2\right)\right]_1^2 = 0$

Table 3.6. Summary of the equations for a non-Newtonian fluid and air system under the influence of a normal electric field after the normal mode expansion.

For the first fluid at $-1 < z_0 < 0$	$Re\left[\omega\hat{v}_{x1} + v_{x0}(ik)\hat{v}_{x1} + \hat{v}_{z1}\frac{dv_{x0}}{dz_0}\right] = -(ik)\hat{p}_1 + [(ik)\hat{\tau}_{xx1} + \frac{d\hat{\tau}_{zx1}}{dz_0}]$
	$Re[\omega\hat{v}_{z1} + v_{x0}(ik)\hat{v}_{z1}] = -\frac{d\hat{p}_1}{dz_0} + [(ik)\hat{\tau}_{xz1} + \frac{d\hat{\tau}_{zz1}}{dz_0}]$
	$(ik)\hat{v}_{x1} + \frac{d\hat{v}_{z1}}{dz_0} = 0$
	$-k^2\hat{V}_1^{(1)} + \frac{d^2\hat{V}_1^{(1)}}{dz_0{}^2} = 0$
	$\hat{\tau}_{xx1} + We\left[\omega\hat{\tau}_{xx1} + v_{x0}(ik)\hat{\tau}_{xx1} + \hat{v}_{z1}\frac{d\tau_{xx0}}{dz_0} - 2(ik)\hat{v}_{x1}\tau_{xx0} - 2\frac{dv_{x0}}{dz_0}\hat{\tau}_{zx1} - 2\frac{d\hat{v}_{x1}}{dz_0}\tau_{zx0}\right] = 2(ik)\hat{v}_{x1}$
	$\hat{\tau}_{xz1} + We\left[\omega\hat{\tau}_{xz1} + v_{x0}(ik)\hat{\tau}_{xz1} + \hat{v}_{z1}\frac{d\tau_{xz0}}{dz_0} - (ik)\hat{v}_{z1}\tau_{xx0} - \frac{dv_{x0}}{dz_0}\hat{\tau}_{zz1}\right] = \frac{d\hat{v}_{x1}}{dz_0} + (ik)\hat{v}_{z1}$
	$\hat{\tau}_{zz1} + We\left[\omega\hat{\tau}_{zz1} + v_{x0}(ik)\frac{d\hat{\tau}_{zz1}}{dx_0} - 2(ik)\hat{v}_{z1}\tau_{xz0}\right] = 2\frac{d\hat{v}_{z1}}{dz_0}$
For the second fluid at $0 < z_0 < Hr$	$-k^2\hat{V}_1^{(2)} + \frac{d^2\hat{V}_1^{(2)}}{dz_0{}^2} = 0$

Table 3.7. Summary of the boundary and interface conditions for a non-Newtonian fluid and air system under the influence of a normal electric field after the normal mode expansion.

At the bottom wall, z_0 = -1	$\hat{v}_{x1} = 0$
	$\hat{v}_{z1} = 0$
	$\hat{V}_1^{(1)} = 0$
At the top wall, z_0=Hr	$\hat{V}_1^{(2)} = 0$
At the interface, $z_0 = 0$	$\hat{v}_{z1} - (ik)v_{x0}\hat{Z}_1 = \omega\hat{Z}_1$
	$\left[(ik)\hat{V}_1^{(j)} + (ik)\hat{Z}_1\frac{dV_0^{(j)}}{dz_0}\right]_1^2 = 0$
	$\hat{q}_1 = \left[\varepsilon^{(j)}\left(-\frac{d\hat{V}_1^{(j)}}{dz_0}\right)\right]_1^2$
	$\omega\hat{q}_1 + v_{x0}(ik)\hat{q}_1 + q_0(ik)\hat{v}_{x1} = S\left(\sigma_r\frac{d\hat{V}_1^{(2)}}{dz_0} - \frac{d\hat{V}_1^{(1)}}{dz_0}\right)$
	$-\hat{p}_1 + \hat{\tau}_{zz1} - 2(ik)\hat{Z}_1\tau_{xz0} - \left[\varepsilon^{(j)}E_b\left(\frac{dV_0^{(j)}}{dz_0}\frac{d\hat{V}_1^{(j)}}{dz_0}\right)\right]_1^2 = (-k^2)\hat{Z}_1$
	$\hat{\tau}_{xz1} + \hat{Z}_1\frac{d\tau_{xz0}}{dz_0} - (ik)\hat{Z}_1\tau_{xx0} - \left[\varepsilon^{(j)}E_b\left(\frac{dV_0^{(j)}}{dz_0}(ik)\hat{V}_1^{(j)} + (ik)\hat{Z}_1\left(\frac{dV_0^{(j)}}{dz_0}\right)^2\right)\right]_1^2 = 0$

It is assumed that the base state is stationary, i.e. v_{x0} and τ_{xx0} are zero. Also, as this work mainly based on micro channel applications, Reynolds number, Re is also taken as zero. Then, $\hat{v}_{z1}$ is found as

$$\hat{v}_{z1} = C_1 e^{kz_0} + C_2 z_0 e^{kz_0} + C_3 e^{-kz_0} + C_4 z_0 e^{-kz_0} \tag{3.94}$$

$\hat{V}_1^{(j)}$ is found from Table 1.6, and Table 1.7 as

$$\hat{V}_1^{(1)} = C_5 \, sinh(kz_0) + C_6 cosh(kz_0) \tag{3.95}$$

$$\hat{V}_1^{(2)} = C_7 \sinh(kz_0) + C_8 \cosh(kz_0) \tag{3.96}$$

The derivation of $\hat{v}_{z1}$ and $\hat{V}_1^{(j)}$ is given in Appendix B. The Equations (3.94)-(3.96), and the equations in Table 3.7 are solved in MAPLE and the effect of various dimensionless numbers, We, Eb, Hr, S, $\varepsilon^{(j)}$, and σ_r are analyzed in the results section.

3.2. A Non-Newtonian Fluid and Air System Under the Influence of a Parallel Electric Field

In this section, the same physical system as in the normal electric field is used except that the electric field is applied parallel to the interface as shown in Figure 3.2.

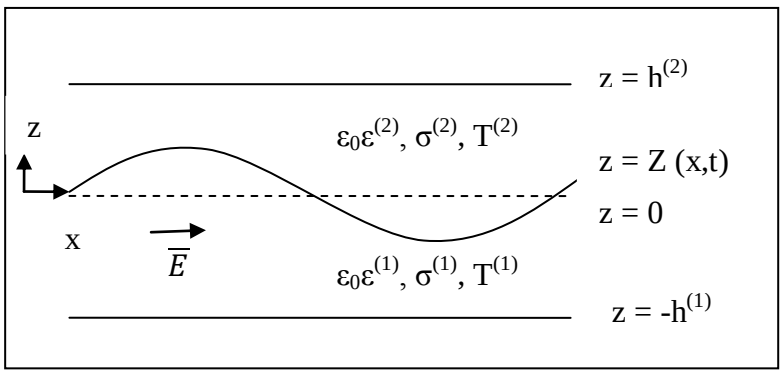

Figure 3.2. Two-phase system under the effect of parallel electric field.

The governing equations are identical to the first case, because the governing equations do not include any term with the electric field. The difference of the parallel field from the normal field is observed at the boundary and interface conditions.

The applied voltage, at x=0, is

$$V^{(j)} = V_b \tag{3.97}$$

and, at x=L, is

$$V^{(j)} = 0 \tag{3.98}$$

The base state voltage potential is found as

$$V_0{}^{(j)} = -\beta x_0 + 1 \tag{3.99}$$

where β is defined as

$$\beta = \frac{h^{(1)}}{L} \tag{3.100}$$

Then, the electric field equation for both fluids, at the base state, are obtained as

$$\underline{E}_0{}^{(j)} = \beta \underline{e}_{x0} \tag{3.101}$$

Equation (3.101) is then substituted into Gauss' law at the base state, and finally surface charge density at the base state is found as

$$q_0 = 0 \tag{3.102}$$

The boundary and interface conditions are linearized, and expanded in normal mode. Then, v_{x0}, τ_{xx0}, and Re are taken as zero as in the first case. The obtained equations are given in Table 3.8.

Table 3.8. Summary of the boundary and interface conditions for a non-Newtonian fluid and air system under the influence of a parallel electric field after the normal mode expansion.

At the bottom wall, $z_0 = -1$	$\hat{v}_{x1} = 0$
	$\hat{v}_{z1} = 0$
	$\frac{d\hat{V}_1^{(1)}}{dz_0} = 0$
At the top wall, z_0=Hr	$\frac{d\hat{V}_1^{(2)}}{dz_0} = 0$
At the interface, $z_0 = 0$	$\hat{v}_{z1} = \omega\hat{Z}_1$
	$\left[\hat{V}_1^{(j)}\right]_2^1 = 0$
	$\hat{q}_1 = \left[\varepsilon^{(j)}\left(-\frac{d\hat{V}_1^{(j)}}{dz_0} + (ik)\frac{dV_0^{(j)}}{dx_0}\hat{Z}_1\right)\right]_1^2$
	$\omega\hat{q}_1 = S\left(\sigma_r\left(\frac{d\hat{V}_1^{(2)}}{dz_0} - (ik)\hat{Z}_1\frac{dV_0{}^{(2)}}{dx_0}\right) - \left(\frac{d\hat{V}_1^{(1)}}{dz_0} - (ik)\hat{Z}_1\frac{dV_0{}^{(1)}}{dx_0}\right)\right)$
	$-\hat{p}_1 + \hat{\tau}_{zz1} + \left[\varepsilon^{(j)}E_b\left(\frac{dV_0{}^{(j)}}{dx_0}(ik)\hat{V}_1{}^{(j)}\right)\right]_2^1 = (-k^2)\hat{Z}_1$
	$\hat{\tau}_{xz1} + \left[\varepsilon^{(j)}E_b\left(\frac{dV_0{}^{(j)}}{dx_0}\frac{d\hat{V}_1{}^{(j)}}{dz_0} - (ik)\hat{Z}_1\left(\frac{dV_0{}^{(j)}}{dx_0}\right)^2\right)\right]_2^1 = 0$

4. RESULTS AND DISCUSSION

In this chapter, the results of the linear stability analysis of both the normal and the parallel field systems are introduced. First, the stability results of a non-Newtonian (UCM) liquid and air system where air is assumed to be hydrodynamically passive are compared with the stability results of a UCM and a Newtonian liquid system. Then, the stability results of the UCM liquid and air system under both the normal and the parallel electric field are compared, and the neutral curves are also obtained. It should be noted that the imaginary part of the dimensionless growth rate turned out to be zero for all cases considered.

4.1. Active versus Passive Fluid and UCM Liquid Under the Effect of Normal Electric Field

The results of the linear stability analysis of the system with a non-Newtonian viscoelastic polymer (UCM fluid) and air under the effect of a normal electric field (See Section 3.1) are introduced. The system parameters are chosen as We=1, Hr=1, $S=10^3$, $\varepsilon^{(1)}=4$, $\varepsilon^{(2)}=3$, Eb=1, and $\sigma_r=0.1$ as in Ersoy's (2011) for comparison. The results of Ersoy (2011) are also given for completeness purposes. The wave number versus the real part of the growth rate, i.e. the dispersion curve is plotted to investigate the system stability.

In Figure 4.1, the Weissenberg number (We) effect on the system stability is compared. This number respresents the elasticity of the fluids. We is varied from 0 to 2.5. The fluid is Newtonian when We is zero, and the elasticity of the polymer increases as the Weissenberg number increases. In Figure 4.1a where the Newtonian fluid is a passive gas, as We increases, the maximum growth rate increases, and the critical wave number remains unaffected. This trend is also observed in Wu and Chou's (2005) work (their Figure 3). However; in Figure 4.1b (Ersoy, 2011), as We increases, the critical wave number increases, and the maximum growth rate decreases.

In Figure 4.2, the effect of the dimensionless electric number, Eb, on the stability of the interface is compared for the two different cases. Eb is directly proportional to the

applied electric field. In both cases (Figure 4.2a, and Figure 4.2b) for this set of parameters, Eb has a destabilizing effect. The systems are stable when Eb is equal to zero and as Eb increases, both systems become unstable. However, the passive fluid case (Figure 4.2a) has a growth rate one order of magnitude bigger than the Newtonian liquid (Figure 4.2b) system.

In Figure 4.3, the effect of the thickness ratio of the fluids is compared. The thickness ratio varies from 0.5 to 2. For this set of parameters, both the maximum growth rate and the critical wave number decrease as the thickness ratio increases for both cases (Figure 4.3a, and Figure 4.3b).

The effect of the conductivity ratio of the fluids in the range of 0.1 to 0.9 is presented in Figure 4.4. As the conductivities of the fluids get closer, the interface becomes more stable for both cases (Figure 4.4a, and Figure 4.4b).

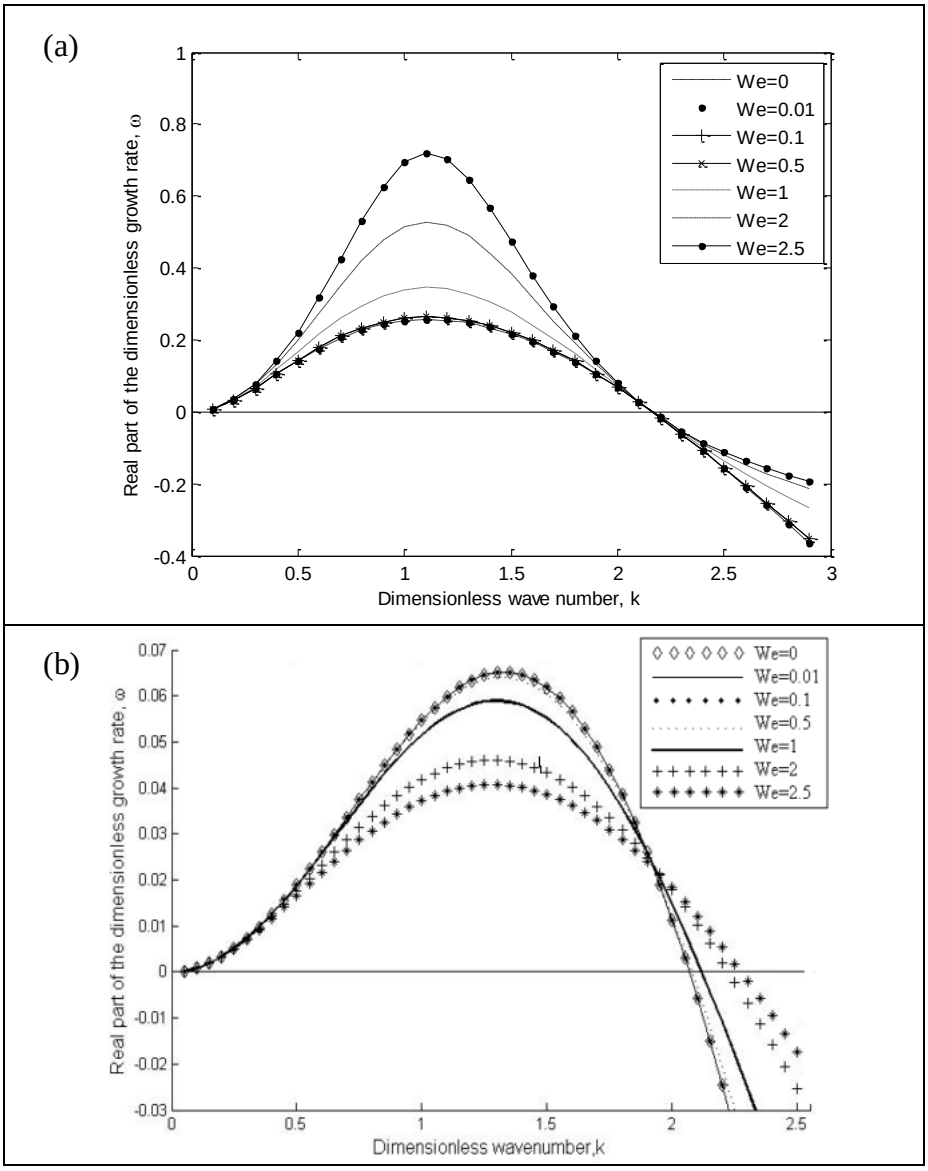

Figure 4.1. Dispersion curves of (a) UCM fluid and air, (b) a Newtonian and a UCM fluid (Ersoy, 2011) system under the effect of an electric field at various Weissenberg numbers.

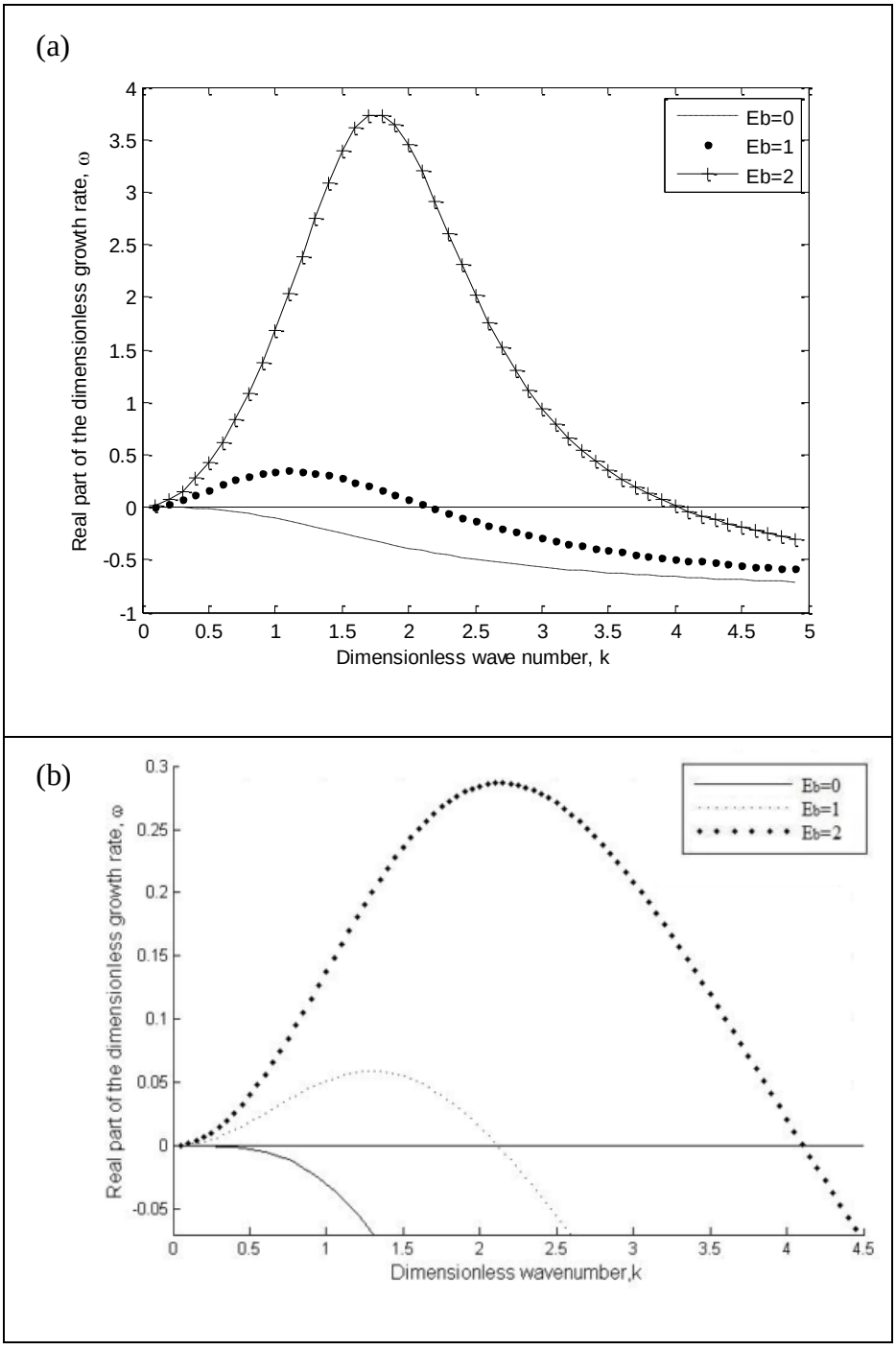

Figure 4.2. Dispersion curves of (a) UCM fluid and air, (b) a Newtonian and a UCM fluid (Ersoy, 2011) system under the effect of an electric field at various dimensionless electric numbers.

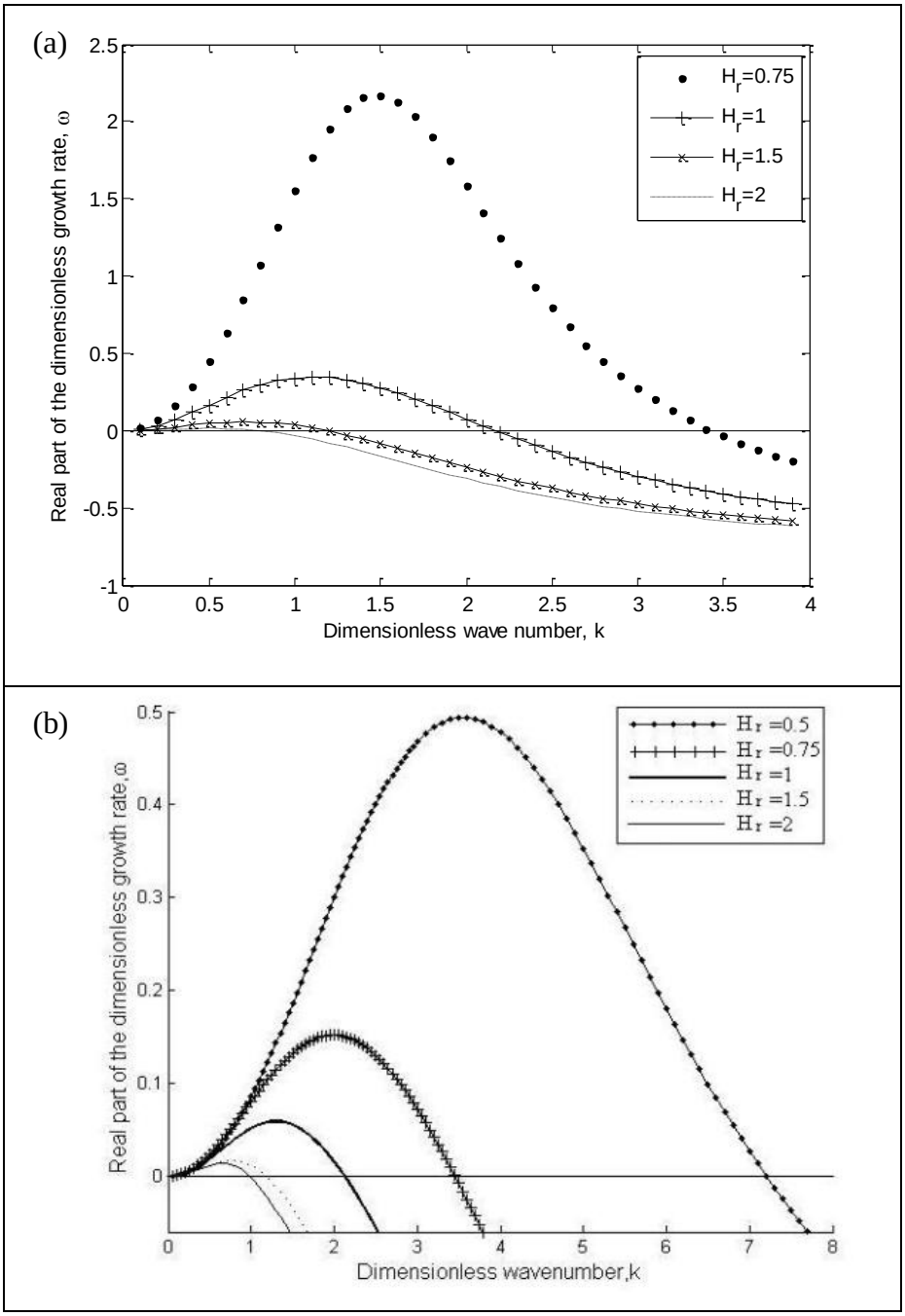

Figure 4.3. Dispersion curves of (a) UCM fluid and air, (b) a Newtonian and a UCM fluid (Ersoy, 2011) system under the effect of an electric field at various thickness ratios.

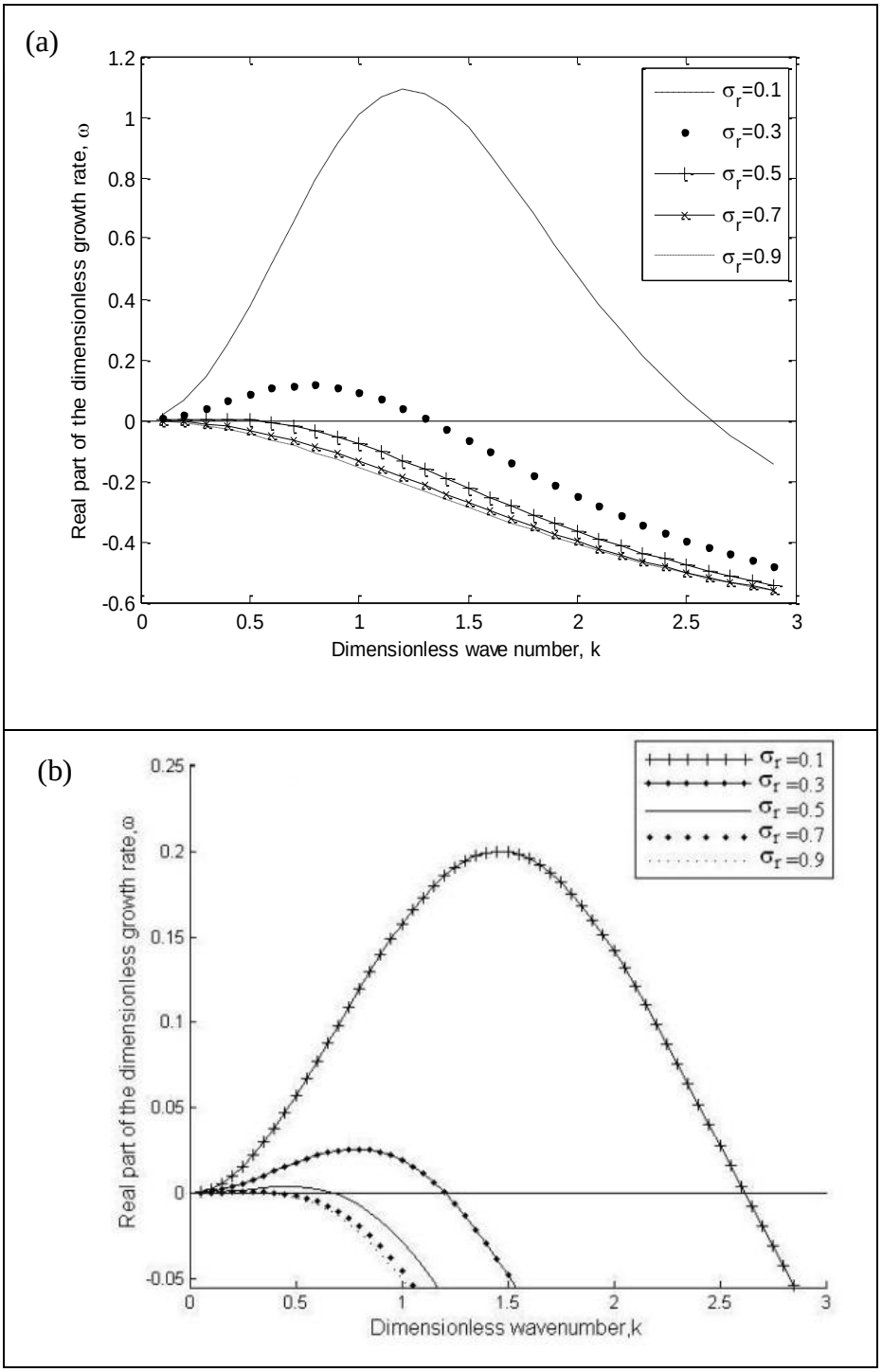

Figure 4.4. Dispersion curves of (a) UCM fluid and air, (b) a Newtonian and a UCM fluid (Ersoy, 2011) system under the effect of an electric field at various conductivity ratios.

4.2. The Effect of the Normal versus the Parallel Electric Field

In this section, the effects of the parallel field and the normal field on the stability of the interface of a viscoelastic polymer (UCM fluid) and air are compared. The parameters used in this section are selected from the literature. The physical and the electrical properties of Poly(methyl methacrylate) (PMMA) (Wu and Chou, 2005), Polydimethylsiloxane (PDMS) (Mark, 2009; Wu, 1989; Hu *et al*., 2010; Kubisz *et al*. 2008), and Polyacrylamide (Purnode and Crochet, 1998; Kopperud and Hansen, 2001; Kreiba, 2000; Bhat and Joshi, 1993) are investigated. These viscoelastic polymers are selected to compare the results with future experimental studies. In Section 4.2.1, the dispersion curves and in Section 4.2.2, the neutral curves will be introduced.

4.2.1. Dispersion Curves

The default parameters are selected considering average values of PMMA's, PDMS's, and Polyacrylamide's physical and electrical properties as We=1, E_b=2, $S=10^7$, Hr=1, $\varepsilon^{(1)}$=2.5, $\varepsilon^{(2)}$=1, $\sigma_r=6*10^{-3}$, $\beta=6.25*10^{-3}$, V_b=500V, $h^{(j)}$=0.25mm.

In Figure 4.5, the effect of We on the system stability is investigated. We is varied from 0 to 2. As seen from Figure 4.5a, increasing We does not change the critical wave number, but slightly increases the maximum growth rates. If a parallel electric field is applied to the system with the same system parameters, Figure 4.5b is obtained. The system is stable for all We considered. As We increases, the system becomes less stable.

The effect of the dimensionless electric number Eb is shown in Figure 4.6. In Figure 4.6a, increasing Eb has a destabilizing effect when the electric field is normal to the interface. The maximum growth rate and the critical wave number increase as Eb increases. In order to compare the effects of the normal and the parallel electric fields, the voltage gradients are kept the same, which is obtained by giving Eb for the normal field and β^2Eb for the parallel field the same values. In Figure 4.6b; however, increasing Eb has a stabilizing effect and the system is always stable for the parallel electric field as expected from Figure 2 of Uguz *et al*. (2008). The given electrical properties fall in region 5 where the parallel electric field has a stabilizing effect (Uguz *et al*., 2008).

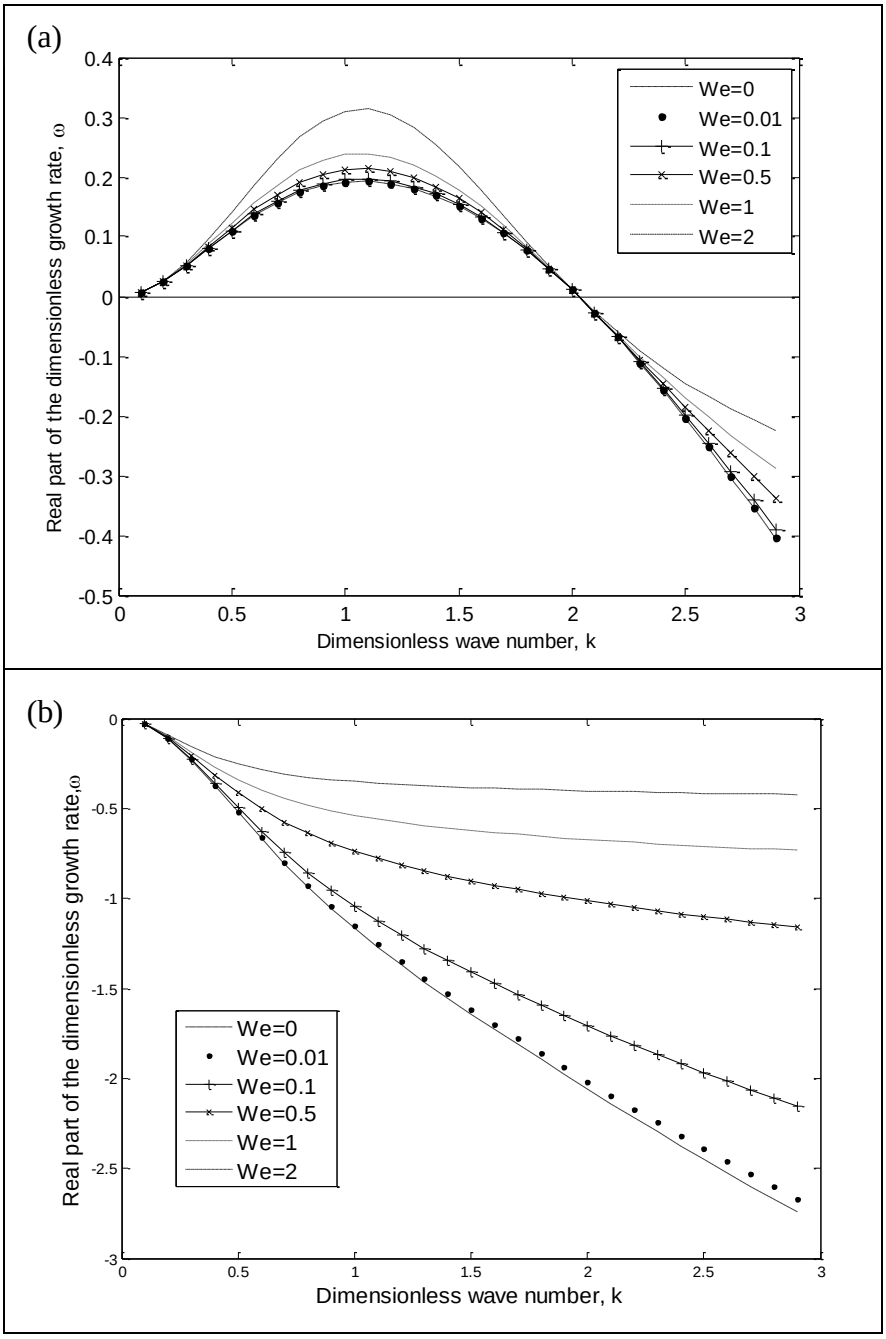

Figure 4.5. Dispersion curves of a UCM fluid and air system under the effect of a (a) normal and (b) parallel electric field at various Weissenberg numbers.

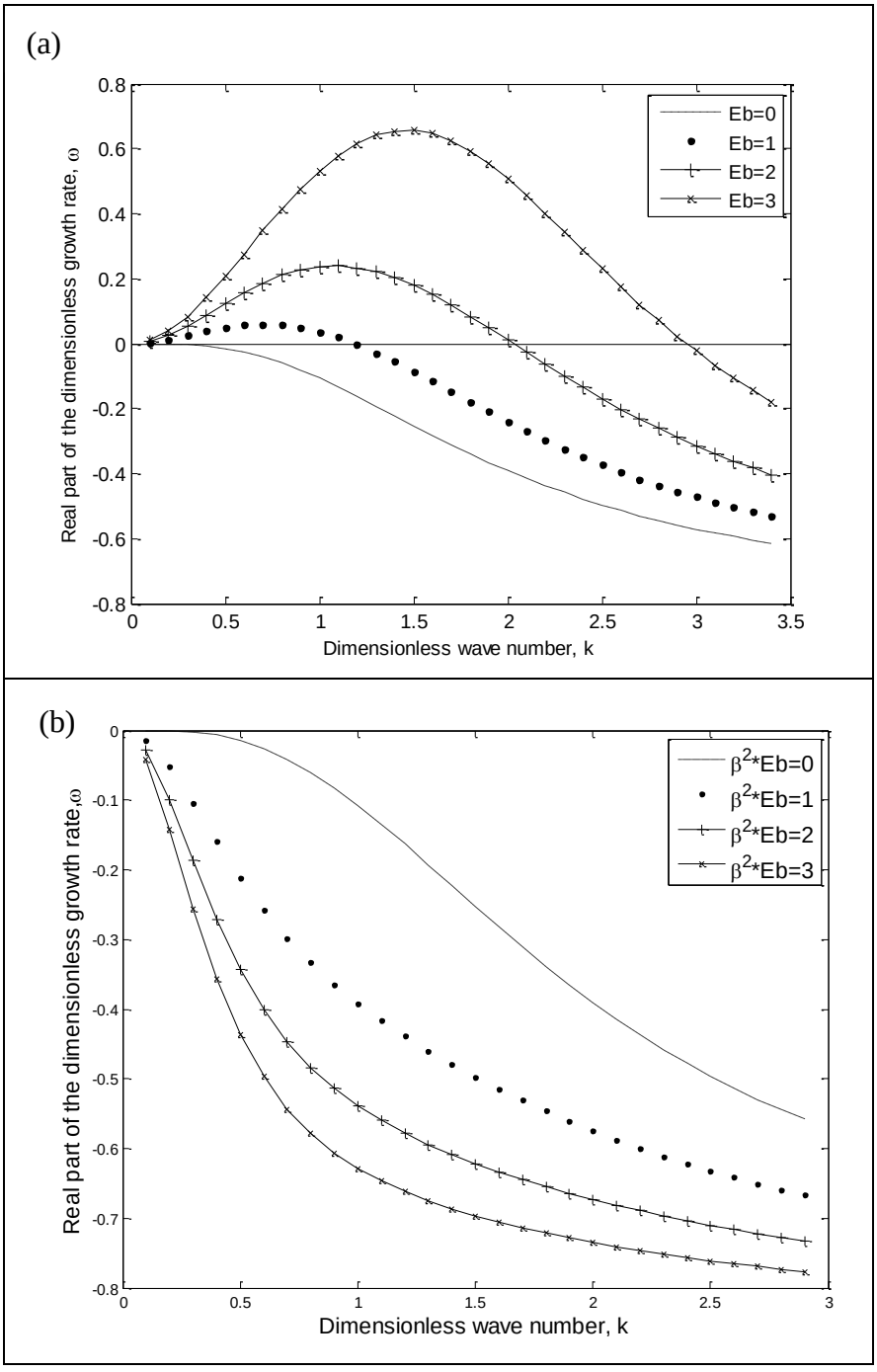

Figure 4.6. Dispersion curves of a UCM fluid and air system under the effect of a (a) normal and (b) parallel electric field at various dimensionless electric numbers.

In Figure 4.7, the effect of the thickness ratio of the fluids which varied between 0.75 to 2. For the default input parameters, the critical wave number and the maximum growth rate decrease as the thickness ratio increases from 0.75 to 2 in Figure 4.7a (for the normal electric field). The effect of the thickness ratio under a parallel electric field is given in Figure 4.7b. Decreasing the thickness ratio has a destabilizing effect for both the

parallel and the normal electric fields. However; for the parallel electric field (Figure 4.7b) the system is stable for this range of thickness ratio, and changing Hr does not have a significant effect on the stability of the system.

In Figure 4.8, the effect of the conductivity ratio is given. The conductivity ratio is altered from 0 to 10^{-3}. It is found that the system responds almost the same for this range, the difference is that the system is unstable for the normal electric field (Figure 4.8a) and stable for the parallel electric field (Figure 4.8b) for the default parameters in this range. In Figure 4.8b, the system becomes unstable when the conductivity ratio is larger than 0.53. However, this would be an unphysical situation as the UCM fluid is much more conductive than air.

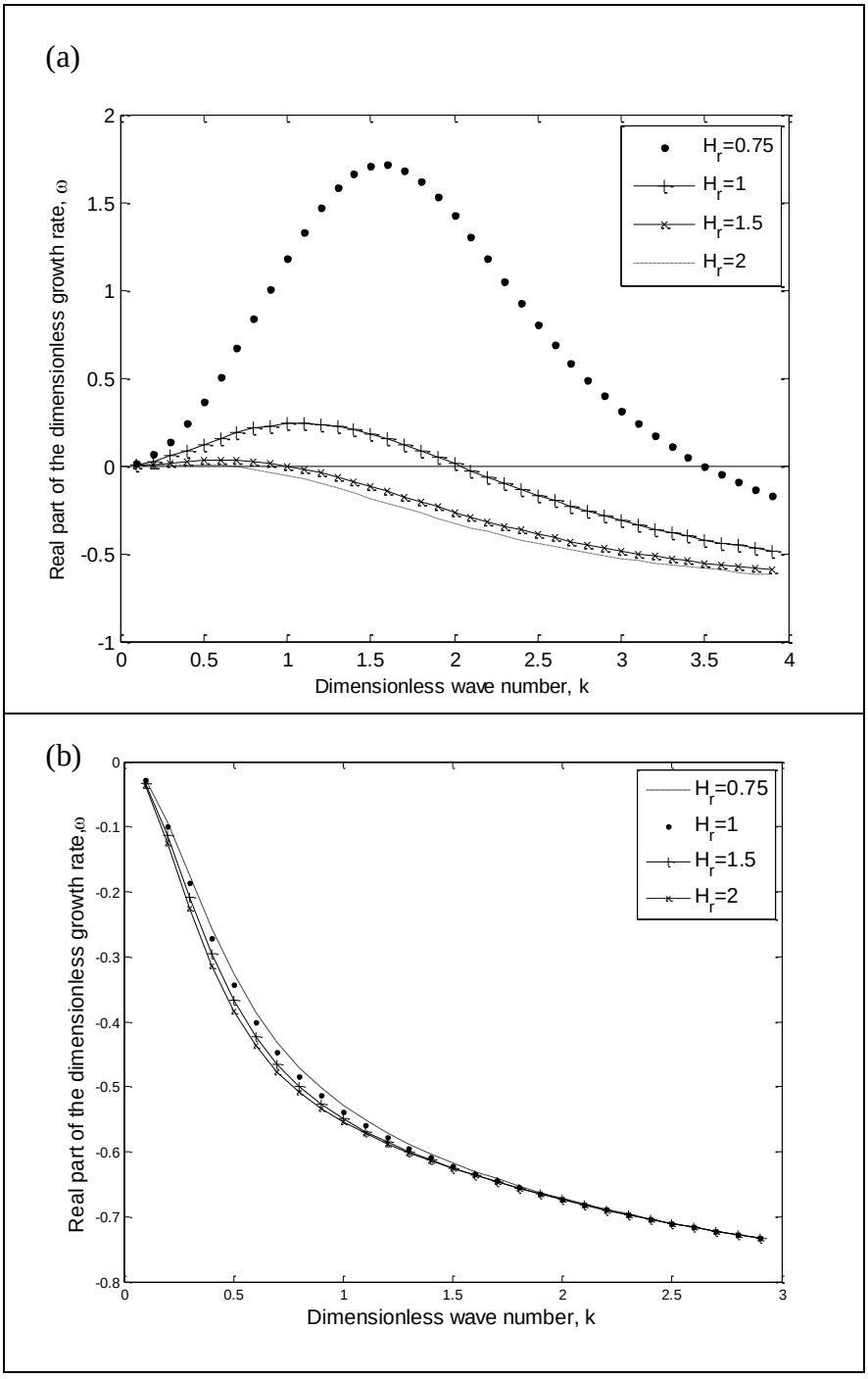

Figure 4.7. Dispersion curves of a UCM fluid and air system under the effect of a (a) normal and (b) parallel electric field at various thickness ratios.

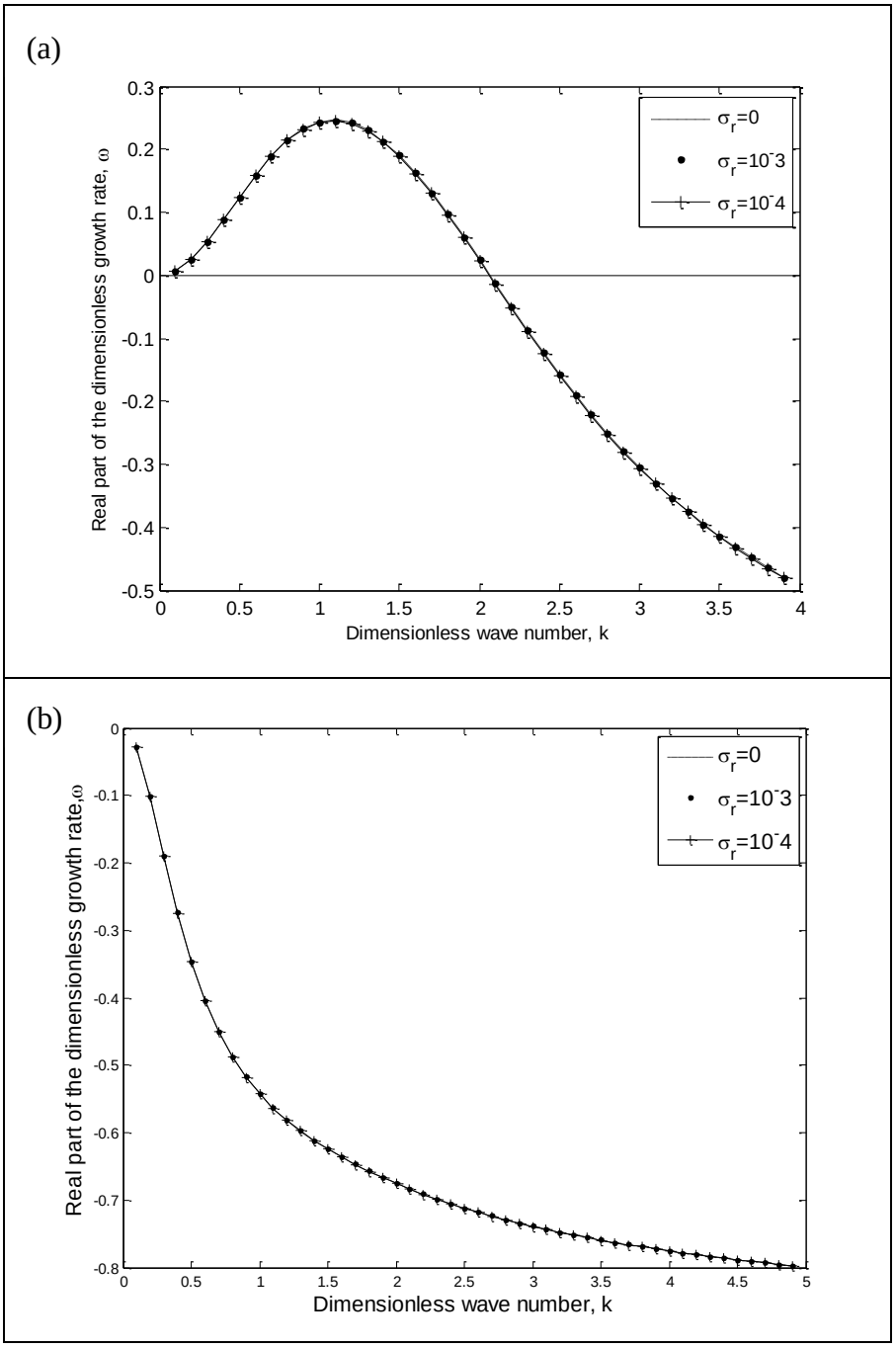

Figure 4.8. Dispersion curves of a UCM fluid and air system under the effect of a (a) normal and (b) parallel electric field at various conductivity ratios.

4.2.2. Neutral Curves for the Normal Electric Field

A neutral stability curve is obtained when the real part of the growth rate is zero, which corresponds to the critical wave number. In this section, the critical wave number,

k_c, versus Weissenberg number, We, the thickness ratio, Hr, and the dimensionless electric number, Eb, are plotted for the default parameters for the normal electric field.

In Figure 4.9, the neutral curve for We is given. It shows that there is only one critical number for all We considered between 0 and 2. When the critical wave number is smaller than 2, the system is unstable to a given infinitesimal disturbance.

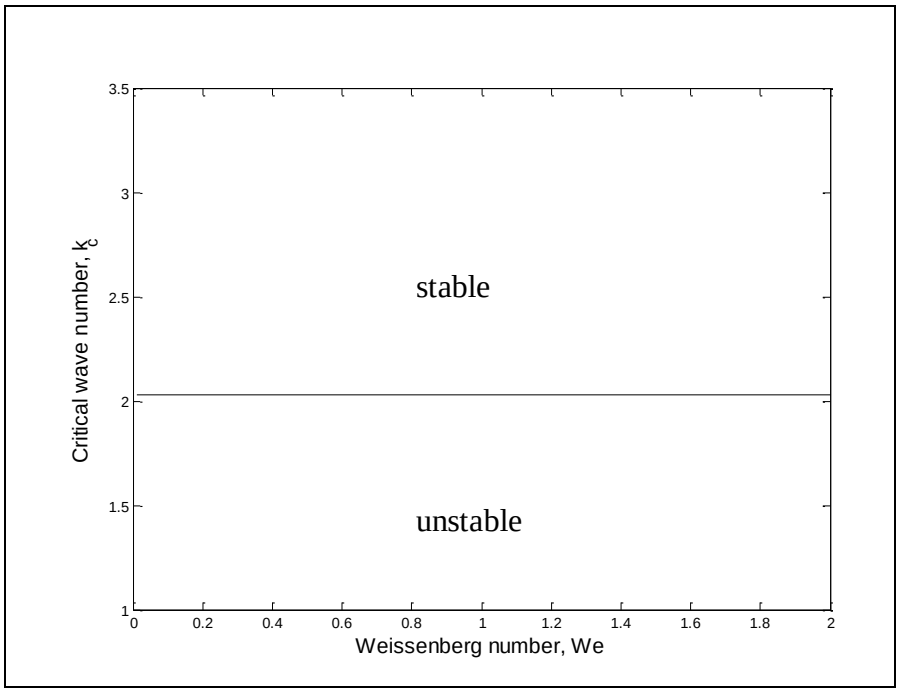

Figure 4.9. Neutral stability curve for the Weissenberg number.

The neutral stability curve for the thickness ratio is given in Figure 4.10. In this figure, it can be seen that there is also one critical wave number for all thickness ratios considered. The stable and the unstable regions are also marked in the figure. As the thickness ratio increases, the critical dimensionless wave number decreases as in Figure 4.7a.

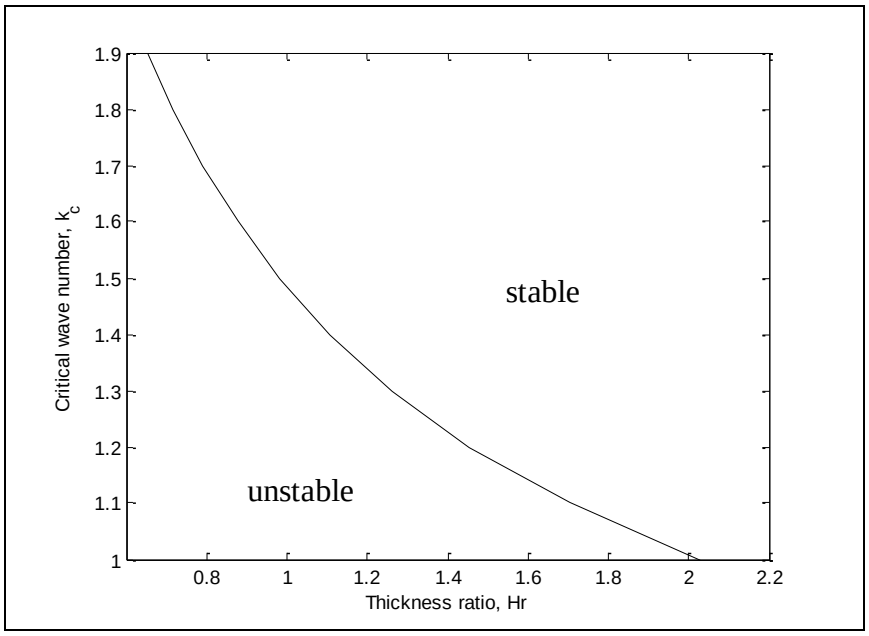

Figure 4.10. Neutral stability curve for the thickness ratio.

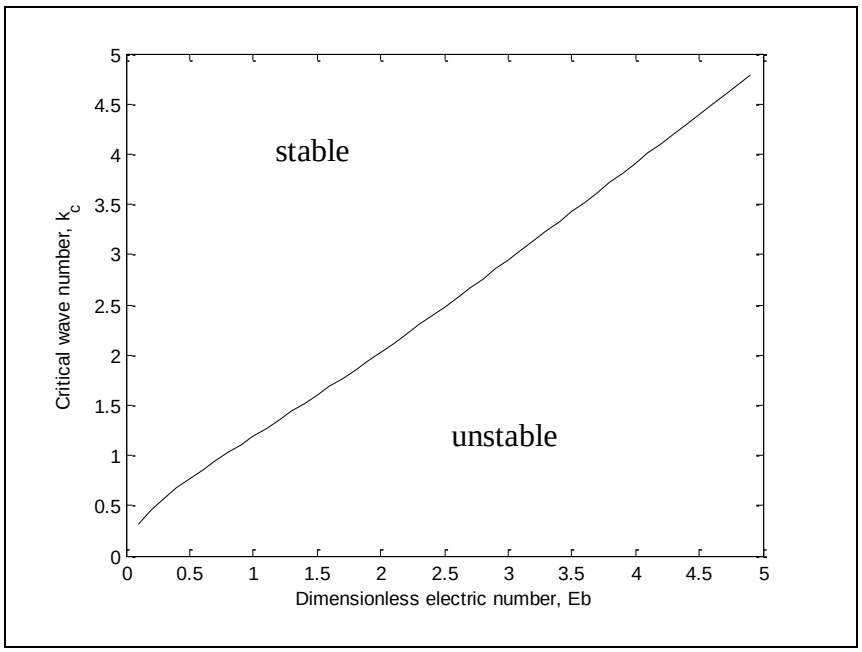

Figure 4.11. Neutral stability curve for the dimensionless electric number.

In Figure 4.11, the neutral stability curve for Eb is given. In contrast to the thickness ratio (Figure 4.10), as Eb increases, the critical wave number also increases for the normal electric field (Figure 4.11). This effect can also be seen in Figure 4.6a.

4.3. Singularity

The stability of the interface between a UCM fluid and air under the effect of both the normal and the parallel electric fields is investigated for a wide range of parameters. For some parameters the growth rate turned out to be very large reaching infinity. In the literature, this behavior is called singularity (Wu and Chou, 2005).

As seen in Figure 4.12, when the thickness ratio is 0.5 for the normal electric field, the solution failed, and a singularity occurred. At H_r=0.5, there is a sudden increase in the growth rate while the wave number is about 0.5, and a sudden decrease occurs afterwards. When a parallel electric field is used for the same parameters, no singularity occurred for the 3 different Eb considered, namely 0, 1, and 2.

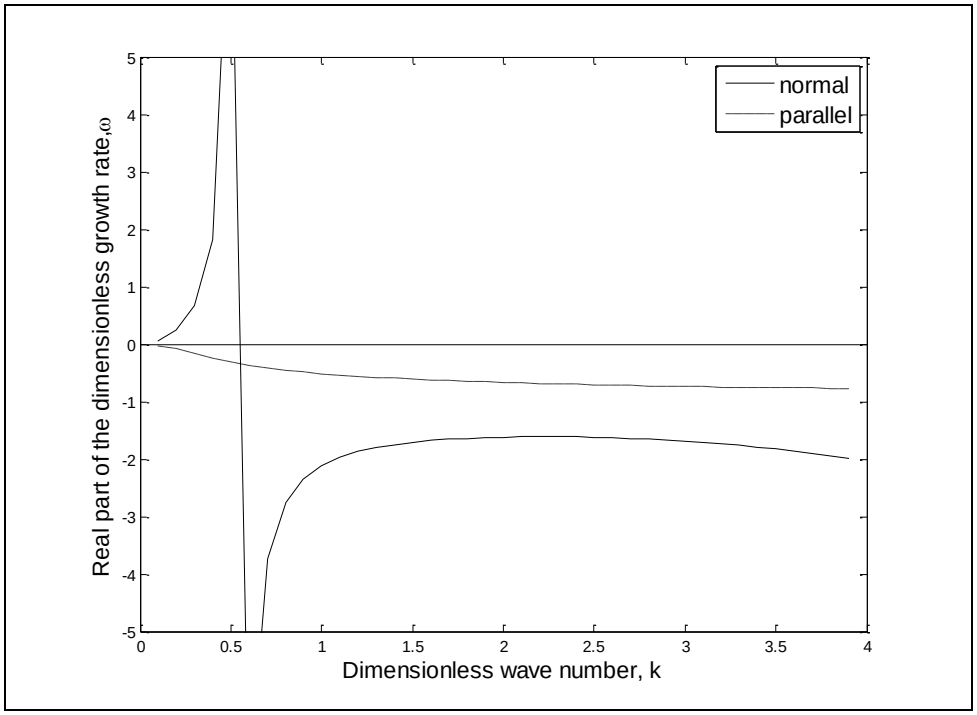

Figure 4.12. Singularity for Hr=0.5 (We=1).

5. CONCLUSION

The linear stability of the interface between a UCM fluid and air in a micro channel under the effect of a normal electric field and a parallel electric field is analyzed. The fluids are assumed to be incompressible, immiscible and leaky-dielectrics. First of all, the effect of a hydrodynamically passive fluid and an active fluid is compared for the normal electric field. Then, the effect of the parallel electric field and the normal electric field is compared for the non-Newtonian (UCM) fluid and air system. The dispersion curves and the neutral curves are obtained.

For the comparison of an active and a passive fluid under the effect of a normal electric field; the dispersion curves are plotted for the same parameters for both cases. The effects of the Weissenberg number, We, the thickness ratio, Hr, the conductivity ratio, σ_r, and the dimensionless electric number, Eb, are investigated. We number has a different effect for two different cases. For the system with an active fluid; increasing We results an increase in the critical wave number, and a decrease in the maximum growth rate. For the system with a passive fluid; increasing We results an increase in the maximum growth rate, and does not affect the critical wave number. Hr, σ_r, and Eb have the same effects for both the passive fluid and the active fluid.

Next, the effect of the normal electric field and the parallel electric field on the stability of the system with a UCM fluid and air is investigated. The effects of We, Hr, $\sigma_{r,}$ and Eb are analyzed for both the normal electric field and the parallel electric field. Increasing We does not change the critical wave number, but slightly increases the maximum growth rates for the normal electric field. The system is stable for this range of We for the parallel electric field. Decreasing the thickness ratio has a destabilizing effect for the normal electric field; however the system is always stable for the parallel electric field, and decreasing the thickness ratio does not have a significant effect on the system stability. The conductivity ratio in the range of 0 to 10^{-3} does not affect the dispersion curves considerably. For the parallel electric field, the system is stable in this range; when the conductivity ratio is larger than 0.53, the system becomes unstable. Increasing Eb has a destabilizing effect for the normal electric field; however it has a stabilizing effect for the

parallel electric field. Note that the applied voltage for the parallel field is 25600 times larger than for the normal field.

The neutral stability curves are also obtained for We, Hr, and Eb. Because the parallel field results are always stable for all dimensionless parameters considered; the neutral stability curves are plotted for the normal electric field. The critical wave number is 2 for all We. The system is unstable if the critical wave number is smaller than 2. It is shown that as Hr increases, the critical dimensionless wave number decreases. For the normal electric field, the neutral stability curve for Eb shows that as Eb increases, the critical wave number also increases.

Finally, for some values of the dimensionless parameters, the solution failed. This singularity occurred when Hr is 0.5 for the normal electric field, for the same ratio the same effect is not observed for the parallel electric field.

6. RECOMMENDATIONS

An experimental study can be carried out and the results can be compared with the theoretical results.

The fluids can be assumed as perfect dielectric or conductive, and another model can be applied.

The singularities can be further investigated for different sets of parameters, and an experiment can be done to understand the reason for this failure.

A non linear stability analysis can be conducted as the linear stability analysis only determines whether the system is stable or not. The fate of the interface can be determined e.g., whether the interface will rupture or not.

Another constitutive equation such as power law can be used instead of the UCM model.

The Reynolds number is taken as zero in this study, the effect of the Reynolds number can be observed without eliminating Reynolds number from the equations.

The stability between a non-Newtonian and a hydrodynamically active Newtonian fluid under the effect of a parallel electric field can be studied, and compared with the normal electric field case (Ersoy, 2011).

APPENDIX A: DERIVATION OF THE INTERFACE VARIABLES

In this appendix; the derivation of interface and boundary variables used in Section 3.1.4.2 are presented.

The unit normal vector is described as

$$\underline{n} = \frac{\nabla f}{|\nabla f|} \tag{A.1}$$

where f is a constant surface, and defined as

$$f = z - Z(x) \tag{A.2}$$

The unit normal vector in Rectangular Cartesian Coordinate System is found as

$$\underline{n} = \frac{\underline{e}_z - \frac{\partial Z}{\partial x}\underline{e}_x}{\sqrt{1 + \left(\frac{\partial Z}{\partial x}\right)^2}} \tag{A.3}$$

By expanding the unit normal vector in Taylor series, the base state and the perturbed state unit normal vector are found

$$\underline{n} = \underline{n}_0 + \varepsilon \underline{n}_1 \tag{A.4}$$

where $\underline{n}_0$ is the base state unit normal vector which is found using Equation (A.3)

$$\underline{n}_0 = \frac{\underline{e}_{z0} - \frac{\partial Z_0}{\partial x_0}\underline{e}_{x0}}{\sqrt{1 + (Z_{x0})^2}} \tag{A.5}$$

where $\frac{\partial Z_0}{\partial x_0}$ is zero, thus reduces to

$$\underline{n}_0 = \underline{e}_{z0} \tag{A.6}$$

$\underline{n}_1$ is the perturbed unit normal vector, defined as

$$\underline{n}_1 = \frac{\partial \underline{n}}{\partial \varepsilon} \tag{A.7}$$

which gives

$$\underline{n}_1 = \frac{0 - \frac{\partial Z_1}{\partial x_0}\underline{e}_{x0}}{\sqrt{1 + \left(\frac{\partial Z_0}{\partial x_0}\right)^2}} \tag{A.8}$$

$$\underline{n}_1 = -\frac{\partial Z_1}{\partial x_0}\underline{e}_{x0} \tag{A.9}$$

The dot product of the unit normal and the unit tangent vector is zero, i.e.,

$$\underline{n} \cdot \underline{t} = 0 \tag{A.10}$$

Thus, the unit tangent vector is found as

$$\underline{t} = \frac{\underline{e}_x + \frac{\partial Z}{\partial x}\underline{e}_z}{\sqrt{1 + \left(\frac{\partial Z}{\partial x}\right)^2}} \tag{A.11}$$

The unit tangent vector is expanded in Taylor series as

$$\underline{t} = \underline{t}_0 + \varepsilon \underline{t}_1 \tag{A.12}$$

The base state unit tangent vector becomes

$$\underline{t}_0 = \frac{\underline{e}_{x0} + \frac{\partial Z_0}{\partial x_0}\underline{e}_{z0}}{\sqrt{1 + \left(\frac{\partial Z_0}{\partial x_0}\right)^2}} \tag{A.13}$$

where Z_{x0} is zero, thus reduces to

$$\underline{t}_0 = \underline{e}_{x0} \tag{A.14}$$

$\underline{n}_1$ is the perturbed unit normal vector, defined as

$$\underline{t}_1 = \frac{\partial \underline{t}}{\partial \varepsilon} \tag{A.15}$$

which gives

$$\underline{t}_1 = \frac{0 + \frac{\partial Z_1}{\partial x_0}\underline{e}_{z0}}{\sqrt{1 + \left(\frac{\partial Z_0}{\partial x_0}\right)^2}} \tag{A.16}$$

$$\underline{t}_1 = \frac{\partial Z_1}{\partial x_0}\underline{e}_{z0} \tag{A.17}$$

The velocity of the interface is expressed as

$$u = \underline{u} \cdot \underline{n} \tag{A.18}$$

where u is defined as

$$u = \frac{f_t}{|\nabla f|} \tag{A.19}$$

which becomes

$$u = \frac{\frac{\partial Z}{\partial t}}{\sqrt{1 + \left(\frac{\partial Z}{\partial x}\right)^2}} \tag{A.20}$$

The base state interface velocity is

$$u_0 = \frac{\partial Z_0}{\partial t_0} = 0 \tag{A.21}$$

and the perturbed state velocity is

$$u_1 = \frac{\partial Z_1}{\partial t_0} \tag{A.22}$$

Twice of the mean curvature of the surface is defined as

$$2H = \frac{\frac{\partial^2 Z}{\partial x^2}}{\sqrt{1 + \left(\frac{\partial Z}{\partial x}\right)^2}^{3/2}} \tag{A.23}$$

At the base state,

$$2H_0 = \frac{\frac{\partial}{\partial x}\frac{\partial}{\partial x}\overbrace{Z_0}^{0}}{\left(\sqrt{1 + \left(\frac{\partial}{\partial x}Z_0\right)^2}\right)^{3/2}} = 0 \tag{A.24}$$

At the perturbed state,

$$2H_1 = \frac{\frac{\partial}{\partial x}\frac{\partial}{\partial x}Z_1}{\left(\sqrt{1 + \left(\frac{\partial}{\partial x}Z_0\right)^2}\right)^{3/2}} \tag{A.25}$$

that reduces to

$$2H_1 = \frac{\partial^2 Z_1}{\partial {x_0}^2} \tag{A.26}$$

APPENDIX B: DERIVATION OF THE VELOCITY AND VOLTAGE

In this appendix, the derivation of $\hat{v}_{z1}$ and $\hat{V}_1^{(j)}$ used in Section 3.1.4.2 is given. After cancelling v_{x0}, τ_{xx0} and Re in the equations in Table 3.6, the following equations are obtained.

$$0 = -(ik)\hat{p}_1 + \left[(ik)\hat{\tau}_{xx1} + \frac{d\hat{\tau}_{zx1}}{dz_0}\right] \tag{B.1}$$

$$0 = -\frac{d\hat{p}_1}{dz_0} + \left[(ik)\hat{\tau}_{xz1} + \frac{d\hat{\tau}_{zz1}}{dz_0}\right] \tag{B.2}$$

$$\hat{\tau}_{xx1} + We[\omega\,\hat{\tau}_{xx1}] = 2(ik)\hat{v}_{x1} \tag{B.3}$$

$$\hat{\tau}_{zx1} + We[\omega\,\hat{\tau}_{zx1}] = \frac{d\hat{v}_{x1}}{dz_0} + (ik)\hat{v}_{z1} \tag{B.4}$$

$$\hat{\tau}_{zz1} + We[\omega\,\hat{\tau}_{zz1}] = 2\frac{d\hat{v}_{z1}}{dz_0} \tag{B.5}$$

$$(ik)\hat{v}_{x1} + \frac{d\hat{v}_{z1}}{dz_0} = 0 \tag{B.6}$$

After taking the derivative of Equation (B.1) with respect to z_0, and multiplying the Equation (B.2) with (ik); subtracting these two equations from each other to eliminate $\hat{p}_1$, the following equation is obtained

$$(ik)\frac{d\hat{\tau}_{xx1}}{dz_0} + \frac{d^2\hat{\tau}_{xx1}}{{dz_0}^2} + k^2\hat{\tau}_{xz1} - (ik)\frac{d\hat{\tau}_{zz1}}{dz_0} = 0 \tag{B.7}$$

From Equations (B.3)-(B.5); $\hat{\tau}_{xx1}$, $\hat{\tau}_{zx1}$, and $\hat{\tau}_{zz1}$ are found as

$$\hat{\tau}_{xx1} = \frac{2(ik)\hat{v}_{x1}}{(1 + We\omega)} \tag{B.8}$$

$$\hat{\tau}_{xz1} = \hat{\tau}_{zx1} = \frac{d\hat{v}_{x1}}{dz_0(1 + We\omega)} + \frac{ik}{(1 + We\omega)}\hat{v}_{z1} \tag{B.9}$$

$$\hat{\tau}_{zz1} = \frac{2}{(1 + We\omega)}\frac{d\hat{v}_{z1}}{dz_0} \tag{B.10}$$

Using the continuity equation, i.e., Equation (B.6); $\hat{v}_{x1}$ is converted into $\hat{v}_{z1}$ in all equations. Then, Equations (B.8)-(B.10) are substituted in Equation (B.7). The following equation is obtained.

$$\frac{d^4\hat{v}_{z1}}{dz_0{}^4} - 2k^2\frac{d^2\hat{v}_{z1}}{dz_0{}^2} + k^4\hat{v}_{z1} = 0 \tag{B.11}$$

Equation (B.11) is solved as follows

$$\left(D^4 + k^4 - 2k^2D^2\right)\hat{v}_{z1} = 0 \tag{B.12}$$

$$\left(D^2 - k^2\right)^2 = 0 \tag{B.13}$$

where D is the differential operator.

$$\hat{v}_{z1} = C_1e^{kz_0} + C_2z_0e^{kz_0} + C_3e^{-kz_0} + C_4z_0e^{-kz_0} \tag{B.14}$$

The governing equation for $\hat{V}_1{}^{(j)}$ from Table 3.6 is

$$-k^2\hat{V}_1{}^{(j)} + \frac{d^2\hat{V}_1{}^{(j)}}{dz_0{}^2} = 0 \tag{B.15}$$

Equation (B.15) is solved as follows

$$\left(D^2 - k^2\right)\widehat{V}_1{}^{(j)} = 0 \tag{B.16}$$

$$(D - k)(D + k)\widehat{V}_1{}^{(j)} = 0 \tag{B.17}$$

$\widehat{V}_1{}^{(j)}$ is found as

$$\widehat{V}_1{}^{(1)} = C_5\, sinh(kz_0) + C_6 cosh(kz_0) \tag{B.18}$$

$$\widehat{V}_1{}^{(2)} = C_7 \sinh(kz_0) + C_8 \cosh(kz_0) \tag{B.19}$$

REFERENCES

Abdella, K., and H. Rasmussen, 1997, "Electrohydrodynamic Instability of Two Superposed Fluids in Normal Electric Fields", *Journal of Computational and Applied Mathematics*, Vol. 78, pp. 33-61.

Balmforth, N.J., R. V. Craster, and C. Toniolo, 2003, "Interfacial instability in non-Newtonian fluid layers", *Physics of Fluids*, Vol. 15, Number 11, pp.3370-3384.

Baygents, J. C., and F. Baldessari, 1998, "Electrohydrodynamic Instability in a Thin Fluid Layer with an Electrical Conductivity Gradient", *Physics of Fluids*, Vol. 10, pp. 301-311.

Belonozhko, D. F., A. I. Grigor'ev, and S. O. Shiryaeva, 1998, "Instability of a charged interface of two immiscible viscous liquids with charge relaxation taken into account", *Technical Physics*, Vol. 43, Number 9, pp. 1023-1027.

Bhat, N. V. and N. V. Joshi, 1993, "Investigation of the Properties of Polyacrylamide-Polyaniline Composite and Its Application as a Battery Electrode", *Journal of Applied Polymer Science*, Vol. 50, pp. 1423-1427.

Bird, R. B., R. C. Armstrong, and O. Hassager, 1987, *Dynamics of Polymeric Liquids*, Vol.1, John Wiley, New York, USA.

Bird, R. B., W. E. Stewart, and E. N. Lightfoot, 2007, *Transport Phenomena*, 2nd ed., John Wiley, New York, USA.

Burcham, C. L., and D. A. Saville, 2000, "The electrohydrodynamic stability of a liquid bridge: microgravity experiments on a bridge suspended in a dielectric gas", *Journal of Fluid Mechanics*, Vol. 405, pp. 37-56.

Castellanos, A., and A. González, 1998, "Nonlinear Electrohydrodynamics of Free Surfaces", *IEEE Dielectrics and Electrical Insulation Society*, Vol. 5, pp. 334-343.

Chhabra, R. P., and J. F. Richardson, 1998, *Non-Newtonian Flow and Applied Rheology*, 2nd ed., Butterworth-Heinemann, Oxford, U.K.

Choi, Y. H., Y. S. Song, and D. H. Kim, 2011, *Mass Transfer-Advanced Aspects*, InTech.

Chou, S. Y., and L. Zhuang, 1999, "Lithographically Induced Self-Assembly of Periodic Polymer Micropillar Arrays", *Journal of Vacuum Science and Technology*, Vol. 17, pp. 3197-3202.

Craster, R. V., and O. K. Matar, 2005, "Electrically Induced Pattern Formation in Thin Leaky Dielectric Films", *Physics of Fluids*, Vol. 17, pp. 032104.1-032104.17.

Darby, R., 1976, *Viscoelastic Fluids*, Dekker, Vol. 9, New York, USA.

Dasgupta, A., P. Sharma, and K. Upadhyayula, 2001, "Micro-Mechanics of Fatigue Damage in Pb-Sn Solder Due to Vibration and Thermal Cycling," *International Journal of Damage Mechanics*, Vol. 10, No. 2. pp. 101-132.

Denn, M. M., 1990, "Issues in Viscoelastic Mechanics", *Annual Review of Fluid Mechanics*, Vol. 22, pp. 13-34.

Deshmukh, A. A., D. Liepmann, and A. P. Pisano, 2000, "Continuous Micromixer with Pulsatile Micropumps", *Berkeley Sensor and Actuator Center*, University of California, pp. 73-76.

Dong, J., Almeida, V. F., and Tsouris, C., 2011, "Formation of Liquid Columns on Liquid–Liquid Interfaces under Applied Electric Fields", *Journal of Colloid and Interface Science*, Vol. 242, pp. 327-336.

El- Sayed, M. F., G. M. Moatimid, and T. M. N. Metwaly, 2011, "Nonlinear Electrohydrodynamic Stability of Two Superposed Streaming Finite Dielectric Fluids in Porous Medium with Interfacial Surface Charges", *Transport in Porous Media*, Vol. 86, pp. 559-578.

Eldabe, N. T., 1987, "Electrohydrodynamic Stability of Two Stratified Power Law Liquids in Couette Flow", *Journal of Mathematical Physics*, Vol. 28, pp. 2791-2800.

Ersoy, G., 2011, "Investigation of the interfacial instability between a newtonian fluid and a polymeric fluid under the influence of an electric field for microfluidics applications", Master Thesis, Bogazici University, Istanbul.

Gambhire, P., and R. M. Thaokar, 2010, "Electrohydrodynamic Instabilities at Interfaces Subjected to Alternating Electric Field", *Physics of Fluids*, Vol. 22, pp 064103.1-064103.16.

Glasgow, I., and N. Aubry, 2003, "Enhancement of Microfluidic Mixing Using Time Pulsing", *Lab on a Chip*, Vol. 3, pp. 114-120.

Guo, L. J., G. J. Li, and X. J. Chen, 2002, "A linear and non-linear analysis on interfacial instability of gas–liquid two-phase flow through a circular pipe", *International Journal of Heat and Mass Transfer*, Vol. 45, pp. 1525-1534.

Harkema, S., E. Schäffer, M. D. Morariu, and U. Steiner, 2003, "Pattern Replication by Confined Dewetting", *Langmuir*, Vol. 19, pp. 9714-9718.

Hoburg, J. F., and J. R. Melcher, 1976, "Internal Electrohydrodynamic Instability and Mixing of Fluids with Orthogonal Field and Conductivity Gradients", *Journal of Fluid Mechanics*, Vol. 73, pp. 333-351.

Hosokawa, K., T. Fujii, and I. Endo, 1999, "Droplet-based nano/picoliter mixer using hydrophobic microcapillary vent", *Micro Electro Mechanical Systems, IEEE 12th*, pp. 388-393.

Howell P.B., D.R. Mott, S. Fertig, C.R. Kaplan, J.P. Golden, E.S. Oran and F.S. Ligler, , 2005, "A microfluidic mixer with grooves placed on the top and bottom of the channel", *Lab on a Chip* 5, pp. 524-530.

Hu, Y., X. Chen, G. M. Whitesides, J. J. Vlassak, and Z. Suo, 2011, "Indentation of polydimethylsiloxane submerged in organic solvents", *Journal of Material Research*, Vol. 26, Number 6, pp. 785-795.

Johns, L. E., and R. Narayanan, 2002, *Interfacial Instability*, Springer-Verlag, New York.

Kath, G. S., and J. F. Hoburg, 1997, "Interfacial electrohydrodynamic instability in normal electric field", *Physics of Fluids*, Volume 20, Issue 6, pp. 912-917.

Khorshidi, B., M. Jalaalb, and E. Esmaeilzadeh, 2011, "Electrohydrodynamic instability at the interface between two leaky dielectric fluid layers", *Colloids and Surfaces A: Physicochemical and Engineering Aspects*, Vol. 380, pp. 207-212.

Kim, D. S., S. W. Lee, T. H. Kwon, and S. S. Lee, 2004, "A barrier embedded chaotic micromixer", *Journal of Micromechanics and Microengineering*, Vol. 14, No.6, pp. 798-805.

Kopaç, M., A. Topuz, and M. Arıkol, 1998, "Viskoelastik Akıskanların İvmeli Akışında Malzeme Parametrelerinin Türev Tipli Bünye Denklemlerine Etkisi", *Turkish Journal of Engineering and Environmental Science*, Vol. 22, pp. 495-502.

Kopperud, H. B., and F. K. Hansen, 2001, "Surface Tension and Surface Dilatational Elasticity of Associating Hydrophobically Modified Polyacrylamides in Aqueous Solutions", *Macromolecules*, Vol. 34, pp. 5635-5643.

Kreiba, A., 2000, "The Rheological Properties of Aqueous Polyacrylamide Solutions", Master Thesis, Concordia University, Canada.

Kubisz, L., A. Skumiel, T. Hornowski, A. Szlaferek, and E. Pankowski, 2008, "The effect of temperature on the electric conductivity of poly(dimethyl siloxane) ferromagnetic gel", *Journal of Physics: Condensed Matter*, Vol. 20, pp. 204118-204123.

Leach, K. A., S. Gupta, M. D. Dickey, C. G. Wilson, and T. P. Russell, 2005, "Electric Field and Dewetting Induced Hierarchical Structure Formation in Polymer/Polymer/Air Trilayers", *Chaos*, Vol. 15, pp. 047506.1-047506.5.

Li, F., O. Ozen, N. Aubry, D. T. Papageorgiou, and P. G. Petropoulos, 2007, "Linear Stability of a Two-Fluid Interface for Electrohydrodynamic Mixing in a Channel", *Journal of Fluid Mechanics*, Vol. 583, pp. 347-377.

Lin, Z., T. Kerle, S. M. Baker, D. A. Hoagland, E. Schäffer, U. Steiner, and T. P. Russel, 2001, "Electric Field Induced Instabilities at Liquid/Liquid Interfaces", *Journal of Chemical Physics*, Vol. 114, pp. 2377-2381.

Liu, R. H., M. A. Stremler, K. V. Sharp, M. G. Olsen, J. G. Santiago, R. J. Adrian, H. Aref, and D. J. Beebe, 2000, "Passive mixing in a three-dimensional serpentine microchannel", *Journal of Microlectromechanical Systems, IEEE,* Vol. 9, No.2, pp. 190-197.

Mahlmann, S. and A. T. Papageorgiou, 2011, "Interfacial Instability in Electrified Plane Couette Flow", *Journal of Fluid Mechanics*, Vol. 666, pp. 155-188.

Mark, J., 2009, *Polymer Data Handbook*, Oxford University Press, Second Edition, New York.

Melcher, J. R., and G. I. Taylor, 1969, "Electrohydrodynamics: A Review of Role of Interfacial Shear Stresses", *Annual Review of Fluid Mechanics*, Vol. 1, pp. 111-146.

Melcher, J. R. and W. J. Schwarz, 1968, "Interfacial Relaxation Overstability in a Tangential Electric-Field", *Physics of Fluids*, Vol. 11, pp. 2604-2616.

Moctar, A.O.E., N. Aubry, and J. Batton, 2003, "Electro-hydrodynamic microfluidic mixer", *Lab on a Chip*, Vol. 3, pp. 273-280.

Mohring, J. U., C. Karcher, and D. Schulze, 2003, “Stability of Liquid Metal Interface Affected by a High-Frequency Magnetic Field”, *International Scientific Colloquium*.

Nguyen, N. T., and Z. Wu, 2005, “Micromixers-a review”, *Journal of Micromechanics and Microengineering*, Vol. 15, pp. 1-16.

Owens, R. G., and T. N. Phillips, 2002, *Computational Rheology*, Imperial College Press, London, U.K.

Ozen, O., N. Aubry, D. Papageorgiou, and P. Petropoulos, 2006a, “Monodisperse Drop Formation in Square Microchannels”, *Physical Review Letters*, Vol. 96, pp. 144501.1-144501.4.

Ozen, O., N. Aubry, D. Papageorgiou, and P. Petropoulos, 2006b, “Electrohydrodynamic Linear Stability of Two Immiscible Fluids in Channel Flow”, *Electrochimica Acta*, Vol. 51, pp. 5316-5323.

Papageorgiou, D. T., and P. G. Petropoulos, 2004, “Generation of interfacial instabilities in charged electrified viscous liquid films”, *Journal of Engineering Mathematics*, Vol. 50, pp. 223-240.

Patankar, N. A., 2011, “Electrokinetic instability: The sharp interface limit”, *Physics of Fluids*, Vol. 23, pp. 14101-14115.

Pease III, L. F., and W. B. Russel, 2002, “Linear Stability Analysis of Thin Leaky Dielectric Films Subjected to Electric Fields”, *Journal of Non-Newtonian Fluid Mechanics*, Vol. 102, pp. 233-250.

Pease, L. F., and W. B. Russel, 2003, "Electrostatically induced submicron patterning of thin perfect and leaky dielectric films: A generalized linear stability analysis", *Journal of Chemical Physics*, Vol. 118, pp. 3790-3804.

Pinarbasi, A., and A. Liakopoulos, 1995, "Stability of two-layer Poiseuille flow of Carreau-Yasuda and Bingham-like fluids", *Journal of Non-Newtonian Fluid Mechanics*, Vol. 57, pp. 227-241.

Purnode, B., and M. J. Crochet, "Polymer solution characterization with the FENE-P model", *Journal of Non-Newtonian Fluid Mechanics*, Vol. 20, pp.1-20, 1998.

Roberts, S. A., and S. Kumar, 2009, "AC Electrohydrodynamic Instabilities in Thin Liquid Films", *Journal of Fluid Mechanics*, Vol. 631, pp. 255-279.

Robinson, J. A., M. A. Bergougnou, G. S. Peter Castle, and I. I. Inculet, 2001, "The Electric Field at a Water Surface Stressed by an AC Voltage", *IEEE Transactions on Industry Applications*, Vol. 37, pp. 735-742.

Salac, D., W. Lu, C. H. Wang, and A. M. Sastry, 2004, "Pattern formation in a polymer thin film induced by an in-plane electric field", *Applied Physics Letters,* Vol. 85, No.7, pp. 1161-1163.

Schäffer, E., T. Thurn-Albrecht, T. P. Russel, and U. Steiner, 2002, "Electrohydrodynamic Instabilities in Polymer Films", *Europhysics Letters*, Vol. 53, pp. 518-523.

Schäffer, E., T. Thurn-Albrecht, T. P. Russell, and U. Steiner, 2000, "Electrically Induced Structure Formation and Pattern Transfer", *Nature*, Vol. 403, pp. 874-877.

Shankar, V., and A. Sharma, 2004, "Instability of the Interface Between Thin Fluid Films Subjected to Electric Field", *Journal of Colloid Interface Science*, Vol. 274, pp. 294-308.

Shankar V., and L. Kumar, 2004, "Stability of two-layer Newtonian plane Couette flow past a deformable solid layer", *Physics of Fluids*, Vol. 16, Number 12, pp. 4426-4442.

Shaqfeh, E. S. G., R.G. Larson, and G.H. Fredrickson, 1989, "The Stability of Gravity Driven Viscoelastic Film Flow at Low to Moderate Reynolds Number", *Journal of Non-Newtonian Fluid Mechanics*, Vol. 31, pp. 87-113.

Stroock, A.D., S.K. Dertinger, G.M. Whitesides, and A. Ajdari, 2002, "Patterning flows using grooved surfaces", *Analytical Chemistry*, Vol. 74, pp. 5306-5312.

Sudarsan, A.P., and V.M. Ugaz, 2006, "Fluid mixing in planar spiral microchannels", *Lab on a Chip*, Vol. 6, pp. 74-82.

Tabeling, P., 2001, "Some basic problems of microfluidics", *14th Australasian Fluid Mechanics Conference*.

Talon, L., and E. Meiburg, 2011, "Plane Poiseuille Flow of Miscible Layers with Different Viscosities: Instabilities in the Stokes", *Journal of Fluid Mechanics*, Vol 686, pp. 484-506.

Thaokar, R. M., and V. Kumaran, 2005, "Electrohydrodynamic Instability of the Interface Between Two Fluids Confined in a Channel", *Physics of Fluids*, Vol. 17, pp. 084104.1-084104.20.

Tomar, G., V. Shankar, and A. Sharma, 2007, "Electrohydrodynamic instability of a confined viscoelastic liquid film", *Journal of Non-Newtonian Fluid Mechanics*, Vol.143, pp. 120-130.

Uguz, A. K., and N. Aubry, 2008, "Quantifying the Linear Stability of a Flowing Electrified Two-Fluid Layer in a Channel for Fast Electric Times for Normal and Parallel Electric Fields", *Physics of Fluids*, Vol. 20, pp. 092103.1-092103.10.

Uguz, A.K., O. Ozen, and N. Aubry, 2008, "Electric field effect on a two-fluid interface instability in channel flow for fast electric times", *Physics of Fluids*, Vol. 20, pp. 031702.1-031702.4.

Whitesides, G. M., 2006, "The origins and the future of microfluidics", *Nature*, Vol 442, pp. 368-373.

Wilkinson, W. L., 1960, *Non-Newtonian Fluids*, Pergamon Press, New York, USA.

Wu, L., and S. Y. Chou, 2005, "Electrohydrodynamic instability of a thin film of viscoelastic polymer underneath a lithographically manufactured mask", *Journal of Non-Newtonian Fluid Mechanics*, Vol. 125, pp. 91-99.

Wu, S., J. Bandrup, E. H. Immergut, 1989, *Polymer Handbook*, Wiley-Interscience, New York, pp. 414-426.

Yiantsios, S. G., and B. G. Higgins, 1988, "Linear stability of plane Poiseuille flow of two superposed fluids", *Physics of Fluids*, Vol. 31, pp. 3225-3339.